

Simulation of a pulsed CO₂ plasma based on a six-temperature energy approach

I. Tsonev^{1*}, O. Biondo^{1,*}, A. Bogaerts¹

¹Research group PLASMANT, University of Antwerp, Department of Chemistry, Universiteitsplein 1, BE-2610 Wilrijk-Antwerp, Belgium.

* Shared first authors

Abstract

Recent time-resolved measurements of gas and vibrational temperatures in pulsed glow discharges have fostered the development and validation of detailed kinetic models to understand the underlying heating dynamics. The models published so far have been successful in identifying the fundamental processes underlying vibrational and gas heating in pure CO₂ discharges; however, this has come at the cost of including vibrational kinetics with thousands of reactions. This makes these models not compatible with self-consistent computational fluid dynamics (CFD) codes, which are needed to develop new plasma reactors operating at high pressures or with complex flow patterns and capture the relevant dynamics in multi-dimension. In this work, we solve separate energy balance equations for the asymmetric and symmetric vibrational modes of CO₂, as well as for the vibrational modes of CO and O₂, the gas temperature, and the electron temperature, making it a six-temperature (6T) plasma model. This eliminates the need to include a vast array of vibrational levels as separate species, drastically reducing the number of reactions in the model. The model is compared with experimental measurements conducted in a pulsed CO₂ glow discharge at 6.7 mbar. Excellent agreement is observed for the temporal evolution of the

vibrational and gas temperatures, confirming that our approach is suitable for modeling systems under significant non-equilibrium conditions, paving the way for coupling detailed CO₂/CO/O₂/O kinetics with CFD codes.

Keywords

vibrational excitation, CO₂ conversion, gas heating, non-thermal plasma, glow discharges, pulsed discharges

1. Introduction

In view of limiting the global temperature rise to 1.5 °C, closing the carbon cycle and electrifying the industry, particularly in the production of fuels and valuable chemicals, pose significant challenges. In effect, the industrial sector is considered the most difficult to electrify, due to a combination of factors, including diverse end-uses, cost sensitivity, high-temperature processes, and continuous operational requirements [1]. The global demand of chemicals continues to grow, making the chemical industry the third-largest source of greenhouse gas emissions today [2]. Therefore, it is crucial to find solutions to replace fossil fuels with renewable electricity as the primary source for process energy [3].

In this regard, plasma-based CO₂ conversion emerges as a versatile and promising technology. Particularly, plasma offers high process versatility, allowing for various types of reactions, including CO₂ splitting and combinations with the conversion of other gases (*e.g.*, CH₄, H₂, H₂O) [4]. Since plasma reactors are powered by electricity, and can quickly be switched on/off, the

technology can easily be combined with different forms of renewable energy sources [5]. Additionally, plasma is typically associated with low investment and operational costs [6], does not require expensive materials, such as rare-earth metals, and can be scaled up for larger applications [7].

The latter is a rather critical point on which the plasma community is now focusing, given that the other features listed have been established. Indeed, the industrial application of plasma for gas conversion faces hurdles, mainly because its energy efficiency needs to be further improved [4].

A key factor in improving efficiency is identifying the fundamental processes underlying CO₂ conversion in a plasma, especially those leading to splitting with minimal energy consumption, and optimizing the reactor design accordingly. For decades, research suggested that the potential of plasma technology lies in the ability to selectively excite the asymmetric stretching mode of the CO₂ molecule, which is believed to lower the activation energy for CO₂ dissociation and thereby increase the energy efficiency of the process [8]. However, uncertainties remain regarding the utilization of the asymmetric stretching mode as an efficient dissociation mechanism. The main reason for this is the lack of detailed experimental data of the temporal dynamics of its excitation, along with that of the dissociation products of CO₂, *i.e.* CO and O₂.

Indeed, time-resolved vibrational temperature profiles are crucial to validate the existing kinetic models. Only recently, glow discharge reactors with power pulsing have been developed for this purpose [9,10]. Specifically, Rivallan *et al.* [9] investigated the temporal evolution at the microsecond timescale of the infrared spectra in the range of 4000-1200 cm⁻¹ with a Fourier-transformed infrared (FTIR) spectrometer during the active phase of an air-CO₂ discharge, in the 1-15 mbar range. The analysis indicated that the recorded spectra were greatly affected by the discharge in the 2400-2200 cm⁻¹ region, where the asymmetric stretching mode of CO₂ falls.

Subsequently, Klarenaar *et al.* [10] extended the time-resolved analysis to the densities of the levels of the symmetric stretching and bending modes of CO₂, which are strongly coupled into one effective vibrational mode due to Fermi resonance [11]. In addition, the authors introduced the measurements of the vibrational levels of CO, produced in the discharge, as well as the rotational temperature, which can be assumed in equilibrium with the translational temperature due to the extremely fast rates of rotational relaxation for CO₂ [12,13]. Therefore, Klarenaar *et al.* [10] were able to monitor the temporal evolution of four different temperatures, namely the temperature of the asymmetric stretching mode (T_3), the symmetric levels of CO₂ (*i.e.* coupled symmetric stretching and bending modes, T_{12}), CO vibrations (T_{CO}) and the gas (T_g), in a CO₂ discharge at 6.7 mbar and an applied current of 50 mA. The accuracy of the time-dependent measurements of T_g by means of FTIR spectroscopy was later confirmed with rotational Raman spectroscopy [14], which enabled also spatially resolved measurements, confirming the hypothesis that T_g is constant along the line-of-sight of the FTIR measurements. Similarly, Klarenaar *et al.* [14] validated the vibrational temperatures measured by [10], relating the rotational Raman spectra of CO₂ to the vibrational temperatures through the vibrationally averaged nuclear degeneracies [15]. The comparison between FTIR and rotational Raman spectroscopies was further continued in [16], with a focus on the excitation of the asymmetric stretching mode within the range of 1.3-6.7 mbar and a discharge current of 10-50 mA. More recently, Damen *et al.* [17] performed time-resolved measurements of the vibrational and rotational temperatures with the same reactor of [10,14,16] but with quantum cascade laser (QCL) spectroscopy as diagnostic tool. Compared to FTIR, QCL spectroscopy allows measurements with a smaller instrumental broadening and higher temporal resolution. On the other hand, the asymmetric stretching mode is not Raman active and therefore T_3 cannot be inferred directly from rotational Raman spectroscopy. Moreover, Damen and co-

authors investigated the effect of N₂ [17] and H₂O [18] addition to the vibrational kinetics of CO₂ and its dissociation, while the influence of O₂ was studied by Vervloedt *et al.* [19] in the same pulsed glow discharge setup.

The extensive characterization of the temporal evolution of vibrational temperatures in pulsed glow discharges provides the ideal framework for benchmarking global kinetic models. The high homogeneity of the positive column of a glow discharge [20] allows for the capture of the main kinetic phenomena without relying on numerous approximations for multi-dimensional processes, such as heat transfer to reactor walls and fluid dynamics. Additionally, power pulsing facilitates the study of vibrational excitation and relaxation, which would otherwise quickly reach a steady state and equilibrate with the other degrees of freedom in continuous-mode discharges.

Global kinetic models, also called zero-dimensional (0D) chemical kinetics models, are the computational tool of choice for describing detailed plasma chemistry in complex gas mixtures. These models are particularly useful for studying molecular discharges where multiple products are formed through dissociation and recombination reactions. Moreover, 0D models are quick to develop and execute, allowing them to be complemented with the solution of the electron Boltzmann equation and detailed vibrational kinetics without significantly increasing computational time and effort [21,22]. In this context, state-to-state (STS) models have been developed to simulate the time-dependent evolution of the densities of numerous vibrational states, which are treated as individual chemical species. Thus, for each individual state, a continuity equation is solved, with production and loss terms determined by reaction rates.

Specific to CO₂, pioneering works on the development of STS models are [23,24]. Thanks to the detailed scheme for the vibrational chemistry of CO₂, Kozák and Bogaerts [24] demonstrated that conversion could be improved in microwave discharges through stepwise excitation of the

asymmetric stretching mode (also known as the ladder-climbing mechanism) [8,25]. This is due to favorable conditions for electron-impact excitation of the low vibrational energy levels and fast vibration-vibration relaxation towards the higher levels, closer to the dissociation limit of the molecule. In contrast, it was also reported in [24] that plasma with strong non-equilibrium between electrons and heavy particles, such as dielectric barrier discharges (DBDs), promote dissociation through channels with much higher energy thresholds than the ladder-climbing mechanism, such as electronic excitation, thereby reducing the associated energy efficiency. These findings motivated further developments of STS 0D models, focusing on vibrational excitation in plasmas with mild deviations from equilibrium [26–28]. In these plasmas, also known as “warm” plasmas, the electron temperature typically exceeds the vibrational temperatures, which are higher than the gas temperature. The STS 0D models developed up to now suggested that the ladder-climbing mechanism can have a beneficial effect on the reactor performance.

Notwithstanding the remarkable effort, the aforementioned detailed STS 0D models lack direct validation with experimental results. This can be ascribed to a fundamental feature often observed in “warm” plasmas, distinguishing them from the low-pressure glow discharges studied by Rivallan *et al.* [9] and Klarenaar *et al.* [10]. This feature is the high degree of spatial inhomogeneity, especially in the radial direction, which is further enhanced by stabilizing swirling flows and microwave absorption patterns in microwave discharges [29]. Due to these complications, direct comparison between experiments and STS 0D models is not possible. Instead, the models can only provide insights that can be linked to certain experimental trends. Thus, while helpful in identifying mechanisms underlying reactor performance *a posteriori*, after the experiments are done, they are not ideal for steering the design of new and improved reactors.

This limitation arises because the predictive power of a model scales with the range of conditions for which it can accurately capture experimental trends.

As “warm” plasmas cannot be used for the validation of 0D models, the N-PRiME group focused on modeling of the low-pressure pulsed glow discharge developed by Klarenaar *et al.* [10]. Particular attention was paid to the “single-pulse” measurement, where a sufficiently high gas flow rate and inter-pulse time were set to ensure full evacuation of the exhaust and replacement with fresh feed gas before the subsequent pulse. These conditions enable to isolate the vibrational kinetics of CO₂ and its potential effects on dissociation without interference from the dissociation products.

The first modelling effort from the N-PRiME group on the “single-pulse” measurement led to two separate contributions, in which the authors modelled the afterglow dynamics [30] and the active phase of the discharge [31]. In the former, they validated a set of vibration-translation (V-T) and vibration-vibration (V-V) energy transfers under plasma-off conditions, where electron kinetics do not play a role and the dynamics are dominated by relaxation processes. In the latter, they added a set of electron impact processes for vibrational excitation and de-excitation. Overall, the model successfully captured the experimental trends for T_3 and T_{12} , although the experimental T_g profile was used as input parameter. Subsequently, Silva *et al.* [32] extended the validation of the kinetic scheme of [30,31] with the self-consistent calculation of T_g in the afterglow of the “single-pulse” measurement of [10]. This confirmed the validity of their vibrational scheme, providing a new reference model for continuing the construction of a fully self-consistent model.

Along with the efforts of the N-PRiME group, two STS 0D models were separately developed for the purpose of reproducing the “single-pulse” measurement of [10]. Kotov [33] employed a reduced vibrational scheme, previously constructed and tested in [34], which included all levels

up to the dissociation limit by grouping them into fewer effective levels. The author was able to qualitatively reproduce the experimental vibrational temperature profiles, although they were overall overestimated. Kotov attributed this discrepancy to the lack of self-consistency of their model, particularly regarding the electron kinetics. Nearly at the same time, Pietanza *et al.* [35] simulated some features of the “single-pulse” experiment with their model, which involved a self-consistent calculation of the electron, vibrational, and heavy particle kinetics. Overall, they obtained good agreement with experiments in terms of vibrational temperatures up to 1 ms, but overestimated the profiles beyond that point. Within the same time frame, the computed electron density was in good agreement with previous estimations [31], but was also overestimated later on. The authors suggested that including some electron loss mechanisms and more symmetric levels of CO₂ could improve the agreement and make the model more complete. These two independent modelling studies underlined the importance of the electron kinetics. Pietanza *et al.* [35] particularly demonstrated that capturing the transient behavior of electron kinetics is essential for a full understanding of the mechanisms underlying the “single-pulse” measurement.

In this regard, Biondo *et al.* [36] attempted a self-consistent calculation of the electron density, along with the estimation of the temporal evolution of the reduced electric field (E/N) from the power profile; the latter was obtained from the current profile and a fixed voltage from [10]. Compared to Pietanza *et al.* [35], Biondo *et al.* [36] observed that E/N should be higher than *ca.* 94 Td throughout the “single-pulse” experiment in order to sustain the discharge, in contrast to previous estimations [10,31]. However, since the voltage profile was not provided for the “single-pulse” experiment, the authors decided to test two extreme cases, *i.e.* 55 Td (as previous estimations) and 90 Td constant throughout the pulse-on time. By including the solution of the gas heat balance equation, Biondo *et al.* [36] could capture the temporal evolution of T_g , together with

that of T_{12} and T_3 , thereby validating their kinetic scheme for gas heating. Particularly, they found that relaxation of electronic states is necessary to obtain good agreement with the experiments at 90 Td, while at lower E/N, the gas heating is underestimated. Therefore, this study confirmed that electron kinetics play a critical role in defining the dynamics of gas heating.

Notwithstanding the high degree of self-consistency reached by this joint effort between the N-PRiME and PLASMANT groups [36], reproducing the “single-pulse” experiment of Klarenaar *et al.* [10] required *ca.* 14000 individual reactions. This extensive kinetic model would not be compatible with a self-consistent computational fluid dynamic (CFD) model, which is needed to develop new plasma reactors, operating at high pressures or with complex flow patterns, to capture the relevant dynamics.

The drawback of extensive kinetic schemes is intrinsic of the STS approach, which requires a state-resolved set of reactions. An alternative approach to avoid computationally expensive reaction sets can be found in the field of laser modelling, as detailed in the book of Smith and Thomson [37]. In this approach, here referred to as the “energy approach“, the solution of the vibrational densities from individual continuity equations (STS approach) is replaced with the solution of only a few energy balance equations, i.e., one for each vibrational manifold. This dramatically reduces the number of chemical species in the model, potentially enabling the coupling of chemical kinetics with multi-physics (CFD) models.

One of the first applications of the energy approach in the context of non-equilibrium CO₂ reactive flows was presented by Kustova and Naghibeda [38]. Their model included multiple CO₂ vibrational modes and the corresponding main energy transitions, while being sufficiently simple and suitable for engineering applications. The authors used the model to obtain non-equilibrium transport coefficients for CFD codes and compared their results with available literature data.

Subsequently, Kustova *et al.* [39] introduced the energy approach to strong non-equilibrium CO₂ flows, to study the structure of shock waves created during Mars atmospheric entry. They developed a three-temperature (T_3 , T_{12} and T_g) model capable of capturing the effects of V-V inter-mode relaxation on bulk viscosity, essential to achieve reasonable solutions in shock wave studies. Recently, Kunova *et al.* [40] made significant efforts to extend and validate the theory underlying the energy approach. A comparison between the STS and energy approach revealed that one can model the vibrational modes of CO₂ and significantly improve the computational cost without any loss of accuracy, thus allowing an efficient implementation into CFD codes. Later, Kustova and Mekhonoshina [41] employed the three-temperature model of [39] to investigate different theories for the calculation of the transition probabilities of intra- and inter-mode vibrational energy transfer. The authors validated the resulting relaxation times against experimental values available in the literature, recommending the use of the forced harmonic oscillator (FHO) model [42] for non-equilibrium flow simulations.

In this work, we make use of the experimental framework provided by Klarenaar *et al.* [10] and the solid computational foundations developed by the PLASMANT [24,26–28,36], N-PRiME [30–32,36] and Saint Petersburg [39–41] groups, to develop a fully self-consistent model capable of reproducing the single-pulse measurement. Particularly, we implement the energy approach in a kinetic plasma model that solves the electron energy balance equation for the electron temperature (T_e), separate vibrational energy balance equations for the asymmetric (T_3) and symmetric ($T_{1,2}$) modes of CO₂, as well as for the vibrational modes of CO (T_{CO}) and O₂ (T_{O2}), and the gas temperature (T_g) balance equation, making it a six-temperature (6T) plasma model. The two-term Boltzmann equation is used to determine the electron energy distribution function (EEDF) and the electron density (n_e) is calculated assuming quasi-neutrality. The successful

comparison of the outcome of our model with the single-pulse experiment confirms the mechanisms for gas heating in pure CO₂ discharges proposed by Biondo *et al.* [36]. Furthermore, this study reveals the dynamic behavior of the electron and ion kinetics, while achieving reasonable agreement with the experimental current profile.

Overall, we achieve satisfactory agreement between our model and the experiments. This confirms that the energy approach is suitable for modelling systems under non-equilibrium conditions, opening up to the coupling of a detailed CO₂/CO/O₂/O kinetics with CFD codes for plasma reactor design and optimization.

2. Computational framework

Our 6-T model is developed and executed in COMSOL Multiphysics® 6.2 [43]. The EEDF is computed self-consistently using the Boltzman solver integrated in the Plasma Module. The rate coefficients of electron-impact reactions are obtained from the integration of the corresponding cross sections over the EEDF. In our model, we include the cross sections for elastic scattering, excitation, ionization and attachment for CO₂ and its dissociation products (CO, O₂, O), whereas for C we only account for elastic scattering. The cross sections are taken from the LXCat database and detailed information on the included processes and references is given in Appendix A1.

2.1. Species included in the model

The species considered in this model are listed in Table 1, and they include 20 neutral species and 18 charged particles.

Table 1. Species included in the model

Neutral species *
CO ₂ (X ¹ Σ _g ⁺), CO ₂ (e ₁), CO ₂ (e ₂), CO(X ¹ Σ _g ⁺), CO(a ³ Π), CO(a ³ Σ ⁺), CO(A ¹ Π) , CO(b ³ Σ ⁺) , CO(B ¹ Σ ⁺) , CO(C ¹ Σ ⁺) , CO(E ¹ Σ ⁺) , O ₂ (X ¹ Σ _g ⁺), O ₂ (a ¹ Δ _g) , O ₂ (b ¹ Σ _g ⁺), O ₂ (A ³ Σ _u ⁺ , C ³ Δ _u , c ¹ Σ _u ⁻), O(³ P), O(¹ D), O(¹ S), O ₃ , C
Charged species
CO ₂ ⁺ , CO ⁺ , O ₂ ⁺ , O ⁺ , O ₃ ⁺ , O ₄ ⁺ , C ⁺ , C ₂ O ₂ ⁺ , C ₂ O ₃ ⁺ , C ₂ O ₄ ⁺ , CO ₄ ⁺ , O ⁻ , O ₂ ⁻ , O ₃ ⁻ , O ₄ ⁻ , CO ₃ ⁻ , CO ₄ ⁻ and electrons.

*For the specific nomenclature of the electronically excited levels, we refer to the LXCat database, from which electron-impact excitation to the listed electronically excited states is taken.

Among the neutral species in the model, two lumped electronic states of CO₂ are included. While the exact composition of these two states is not fully known, there is general consensus about the electronic states present in the energy range between 7 and 10 eV, corresponding to CO₂(e₁), and above 10 eV, corresponding to CO₂(e₂). Both lumped states contain dissociative and radiative states, and some contributing to fast gas heating through collisional quenching [36]. Further details can be found in the work of Pietanza *et al.* [44], which summarizes the relevant literature.

The extensive description of the ion kinetics is of utmost importance to accurately compute the time evolution of the plasma parameters, such as E/N. This is learned from previous modelling studies on low-pressure plasmas and lasers in molecular gases [45–47]. In this regard, it is essential to include ambipolar diffusion losses to the walls, which represent the dominant sink of charged particles in the positive column of glow discharges [48,49]. In our model, the diffusion of charged particles to the walls is described by classical ambipolar diffusion in the presence of negative ions [50]. The mobility of each ion for calculating the corresponding diffusion coefficient is taken from [51], when available, or assumed from similar ions.

2.2. Species continuity equations

For each species except the electrons, the continuity equation is solved:

$$\rho_p \frac{dw_s}{dt} = m\text{flow}_{\text{in}} - m\text{flow}_{\text{out}} + R_s + R_{\text{surf}} \quad (1)$$

where ρ_p is the mass density, and w_s is the mass fraction of species s . $m\text{flow}_{\text{in}}$ is the mass flow feed, $m\text{flow}_{\text{out}}$ is the outlet flow and R_s and R_{surf} are the net rate of change of the species density, based on the gas phase and surface phase reactions, presented in detail in Appendix A1. The pressure in the simulation is kept constant by adjusting the outflow feed. The electron density is computed assuming quasi-neutrality.

The number densities of the vibrational states of CO₂, CO and O₂ are calculated assuming a Boltzmann distribution through the partition function Z . While this assumption is reasonable for the conditions in this study, limitations may arise under conditions for which a non-Boltzmann or Treanor distributions occur. In such cases, our model cannot capture deviations from Boltzmann distributions. However, this limitation does not introduce significant uncertainty on the computed temperature profiles, as the vibrational densities of higher levels in non-equilibrium are either low [24] or exhibit only moderate deviations from a Boltzmann distribution [52].

The partition functions for CO₂, CO and O₂ are presented in equations (2a), (2b) and (2c), respectively.

$$n_{\text{vib, CO}_2}(i_1, i_2, i_3) = \frac{n_{\text{CO}_2^*}(i_2+1)}{Z_{\text{CO}_2}(T_{12}, T_3)} \exp\left(-\frac{i_1 \epsilon_{100}}{k_B T_{12}} - \frac{i_2 \epsilon_{010}}{k_B T_{12}} - \frac{i_3 \epsilon_{001}}{k_B T_3}\right) \quad (2a)$$

$$n_{\text{vib, CO}}(i_{\text{CO}}) = \frac{n_{\text{CO}}}{Z_{\text{CO}}(T_{\text{CO}})} \exp\left(-\frac{i_{\text{CO}} \epsilon_{\text{CO}}}{k_B T_{\text{CO}}}\right) \quad (2b)$$

$$n_{\text{vib, O}_2}(i_{\text{O}_2}) = \frac{n_{\text{O}_2}}{Z_{\text{O}_2}(T_{\text{O}_2})} \exp\left(-\frac{i_{\text{O}_2} \epsilon_{\text{O}_2}}{k_B T_{\text{O}_2}}\right) \quad (2c)$$

where n_{vib} is the vibrational number density as a function of i_1 , i_2 , i_3 , i_{CO} and i_{O_2} , which are the quantum numbers of the symmetric stretching and bending mode, the asymmetric stretching of CO_2 , and of CO and O_2 , respectively. n_{CO_2} , n_{CO} , n_{O_2} and Z_{CO_2} , Z_{CO} , Z_{O_2} are the total number densities and partition functions of CO_2 , CO and O_2 , respectively. ε_1 , ε_2 , ε_3 , ε_{CO} and ε_{O_2} are the energies of the first state of the symmetric stretching, bending mode and asymmetric stretching of CO_2 , and of CO and O_2 , respectively, and k_B is the Boltzmann constant.

Z_{CO_2} is obtained by summation over all vibrational states below the dissociation threshold as follows:

$$Z_{\text{CO}_2}(T_{12}, T_3) = \sum_{(i_1, i_2, i_3)} (i_2+1) \exp\left(-\frac{i_1 \varepsilon_{100}}{k_B T_{12}} - \frac{i_2 \varepsilon_{010}}{k_B T_{12}} - \frac{i_3 \varepsilon_{001}}{k_B T_3}\right). \quad (3)$$

In equations (2a) and (3), the statistical weight s_{i_1, i_2, i_3} is taken into account as i_2+1 . Z_{CO} and Z_{O_2} are computed analogously to equation (3).

The energy of the vibrational modes as function of temperature was calculated as:

$$E_{T_{1,2}}(T_{12}) = \sum_{i_1 i_2 i_3} (i_1 \varepsilon_{100} + i_2 \varepsilon_{010}) n_{\text{vib}}(i_1, i_2, i_3) \quad (4a)$$

$$E_{T_3}(T_3) = \sum_{i_1 i_2 i_3} (i_3 \varepsilon_{001}) n_{\text{vib}}(i_1, i_2, i_3) \quad (4b)$$

$$E_{T_{\text{CO}, \text{O}_2}}(T_{\text{CO}, \text{O}_2}) = \sum_{i_{\text{CO}, \text{O}_2}} (i_{\text{CO}, \text{O}_2} \varepsilon_{\text{CO}, \text{O}_2}) n_{\text{vib}, \text{CO}, \text{O}_2}(i_{\text{CO}, \text{O}_2}) \quad (4c)$$

The heat capacity per molecule of the vibrational degrees of freedom C_{p, T_v} is calculated as the derivative of the vibrational energy (from Eqs (4a-c)) with respect to the vibrational temperature:

$$C_{p, T_v} = \frac{dE_{\text{vib}}(T_v)}{dT_v} \quad (5)$$

2.3. Modeling the electrical circuit

Klarenaar *et al.* [10] did not report on the time evolution of the voltage during the single-pulse experiment. The measurement of the voltage is critical to calculate the power input as a function of time for the simulation. In effect, Damen *et al.* [17] showed that the voltage cannot be assumed constant and presents a significant spike at the onset of the pulse, in order to ionize the gas. Therefore, we couple the Plasma Module with the Electrical Circuit interface to compute the power, using the experimental current profile as a current source. To do so, the plasma is assumed a resistor in a circuit connected to a ballast resistor (50 k Ω) in series, with a capacitor (10 pF) in parallel. Thus, the plasma resistance is obtained from:

$$R = \frac{L_{\text{plasma}}}{(n_e \mu_e q_e) \pi R_{\text{plasma}}^2} \quad (6)$$

where n_e is the electron density, μ_e the electron mobility, and q_e the elementary charge. The voltage is then estimated based on R . Experimentally, Klarenaar *et al.* [10] used a voltage-regulated power supply instead of a current source. Moreover, we note that the ballast resistance used is not large enough to provide a constant current of 50 mA. Consequently, the plasma resistance together with the ballast resistance determines the current passing through the system. Therefore, we choose to use the experimentally reported current source as an input to the simulation in order to avoid numerical instabilities during the solution.

2.4. Energy balance equations

The electron energy balance equation is solved to obtain the average electron energy $\bar{\epsilon}_e$:

$$\frac{d(n_e \bar{\epsilon}_e)}{dt} = S_{en} + Q_{\text{circuit}} \quad (7)$$

where n_e is the electron density, S_{en} is the average energy lost per collision and Q_{circuit} is the deposited power, computed with Ohm's law.

Each of the vibrational temperatures included in this model (T_{12} , T_3 , T_{CO} and T_{O2}) are calculated through separate energy balance equations. This model represents an evolution of the state-to-state approach. While we still use individual excitation and relaxation rates, these are employed to calculate the energy production or loss rates associated with each transition (then summed to give the total energy rates), rather than the vibrational density. The latter, on the other hand, is calculated from the partition function by assuming a Boltzmann distribution within each manifold, as described earlier in Section 2.2. We note that loss and gain in the vibrational energy balance equations due to chemical reactions are not included, as these reactions are orders of magnitude slower than vibrational relaxation for the conditions studied. However, chemical-vibrational coupling should be accounted for to improve accuracy when chemical kinetics play a larger role, such as for the multi-pulse experiment by Damen *et al.* [17]. Future developments will therefore incorporate this coupling as described in [53,54]. For T_{12} , the energy balance equation takes the form of:

$$n_{\text{CO}_2} \cdot \frac{de_{v,T_{12}}}{dt} = Q_{eV} + Q_{VVT} - Q_{VT_{12}} - Q_{\text{cond}T_{12}} - Q_{\text{feed}T_{12}} \quad (8)$$

where $e_{v,T_{12}}$ is the energy deposited into the symmetric levels of CO_2 , Q_{eV} is the energy deposited through collisions with electrons, i.e., the net energy due to superelastic collisions, Q_{VVT} includes the energy transferred from the asymmetric stretching mode to the symmetric levels through intramolecular vibration-vibration-translation (V-V-T) relaxation, but also inter-molecular V-V-T relaxation between T_{O2} and T_{12} . The rate coefficients used in this work are presented in Appendix

A2. V-V-T relaxation differs from V-V relaxation because the energy of the initial vibrational levels does not coincide with that of the final levels, and therefore part of the vibrational energy is lost to translational degrees of freedom [36]. The latter part is not included in Q_{VVT} in (8), but it will be included in the energy balance equations of T_3 , T_{O_2} and T_g .

$Q_{\text{cond}T_{12}}$ is the energy transfer to the walls due to conduction:

$$Q_{\text{cond}T_{12}} = 8 \cdot C_{p,T_{12}}(T_{12}) \cdot D_{\text{CO}_2}(T_g) \cdot \frac{T_{12} - T_{12,\text{wall}}}{R^2} \quad (9)$$

where $C_{p,T_{12}}$ is the heat capacity of the symmetric levels of CO_2 at constant pressure, D_{CO_2} is the diffusion coefficient of CO_2 , $T_{12,\text{wall}}$ is the temperature of the symmetric levels at the reactor walls, and R is the reactor radius. The factor 8 appears because of averaging over the cross section of the reactor, indicating that the equation is an energy balance equation for the average temperature in the plasma. If the averaging is not performed, the factor changes to 4, which then represents the centerline temperature in the reactor assuming a parabolic temperature profile [55]. More details about the choice of this factor will be given in section 3.1. The conduction term (eq. 9) has the same form for all of the vibrational energy balance equations. This term does not include vibrational deactivation due to collisions with the reactor walls, as it was shown earlier that this cooling process is only appreciable for pressure well below 6.7 mbar [56].

Along with conduction, convective cooling due to the feed gas, Q_{feed} , is included in the energy balance equation (eq. 8):

$$Q_{\text{feed}T_{12}} = \dot{m} \cdot w_{\text{CO}_2} \cdot \frac{H_{T_{12}}(T_{12,\text{feed}}) - H_{T_{12}}(T_{12})}{M_{\text{CO}_2} \cdot V_r} \quad (10)$$

where \dot{m} is the mass flow feed (kg/s), w_{CO_2} and M_{CO_2} are the feed mass fraction and the molar mass of CO_2 , $H_{T_{12}}$ is the energy stored in the symmetric levels of CO_2 and V_r is the reactor volume. The

convection term (eq. 10) has the same form for all of the vibrational and gas energy balance equations.

The energy balance equation for T_3 is similar to that of T_{12} :

$$n_{\text{CO}_2} \cdot \frac{de_{v,T_3}}{dt} = Q_{eV} - Q_{VVT} - Q_{VT_3} - Q_{\text{cond}T_3} - Q_{\text{feed}T_3} \quad (11)$$

In this case Q_{VVT} is a loss term, containing intra-molecular V-V-T relaxation analogously to T_{12} , and inter-molecular V-V-T relaxation with CO and O₂. More details on the terms of eq. 11 are given in the Appendix A2.

The energy balance equation for T_{CO} is defined as follows:

$$n_{\text{CO}} \cdot \frac{de_{v,T_{\text{CO}}}}{dt} = Q_{eV} + Q_{VVT_{\text{CO}_2}} - Q_{VT_{\text{CO}}} - Q_{VVT_{\text{O}_2}} - Q_{\text{cond}T_{\text{CO}}} - Q_{\text{feed}_{\text{CO}}} \quad (12)$$

$Q_{VVT_{\text{CO}_2}}$ is the energy transferred from T_3 , included as $-Q_{VVT}$ in eq. 11, whereas $Q_{VVT_{\text{O}_2}}$ represents a loss term for the energy transferred to T_{O_2} via $\text{CO}(\text{ico}) + \text{O}_2 \rightleftharpoons \text{CO} + \text{O}_2(\text{io}_2)$, with a rate coefficient of $1.66 \times 10^{24} \left[\frac{\text{cm}^3}{\text{s}} \right] \cdot e^{41 - 306 \cdot T_g^{-1/3} + 1126 \cdot T_g^{-2/3}}$ taken from [57]. $Q_{VT_{\text{CO}}}$ involves only one type of transition, $\text{CO}(\text{ico}) + \text{M} \rightleftharpoons \text{CO}(\text{ico}-1) + \text{M}$. The rate coefficient for this transition with $\text{M} = \text{CO}_2$, CO and O₂ is taken from [58,59], whereas the rate coefficient with $\text{M} = \text{O}$ is $5.3 \times 10^{13} \left[\frac{\text{cm}^3}{\text{s}} \right] \cdot \sqrt{T_g} \cdot e^{-1600[\text{K}]/T_g}$ [58].

The last vibrational energy balance equation is that for T_{O_2} :

$$n_{\text{O}_2} \cdot \frac{de_{v,T_{\text{O}_2}}}{dt} = Q_{eV} + Q_{VVT_{\text{CO}}} + Q_{VVT_{T_3}} - Q_{VT_{\text{O}_2}} - Q_{VVT_{T_{12}}} - Q_{\text{cond}T_{\text{O}_2}} - Q_{\text{feed}_{\text{O}_2}} \quad (13)$$

Even in this case, Q_{VVT} is split in multiple terms: two positive terms, $Q_{VVT_{\text{CO}}}$ and $Q_{VVT_{T_3}}$, representing the transfer of heat from T_{CO} and T_3 , respectively, and a loss term, $Q_{VVT_{T_{12}}}$, for the

transfer of energy to T_{12} . These terms are described above. V-T relaxation of O_2 , $Q_{VT_{O_2}}$, is taken from the survey of Blauer and Nickerson [57]. All the other terms in (13) are similar to the previous equations.

Finally, we also solve the energy balance equation of T_g :

$$\rho C_p \frac{dT_g}{dt} = Q_{VT} + Q_{VVT} + Q_g - Q_{condT_g} - Q_{feedT_g} \quad (14)$$

where ρ is the gas density, C_p is the mixture-averaged gas heat capacity, subtracted of the heat capacity of the vibrational manifolds (see eq. (8-13) at thermal equilibrium, i.e. for the vibrational temperatures equal to T_g , Q_g is the heat released from the reactions in the plasma and the Joule heating of the electrons. In contrast to the conduction term in the vibrational energy balance equations, Q_{condT_g} uses the thermal conductivity k_g instead of the product $C_p \cdot D_m(T_g)$. k_g is the mixture-averaged thermal conductivity, calculated as:

$$k_g = 0.5 \left(\sum_i x_m k_m + \frac{1}{\sum_m x_m / k_m} \right) \quad (15)$$

where x_m is the molar fraction of species m , and k_m is the thermal conductivity of species m . k_m is net of the vibrational contributions to the thermal conductivity, which are included in eq. (8,-10-13). In order to include only the translational and rotational contributions for the molecules for which separate vibrational energy balance equations exist, we introduce the following calculation from Thomson [60], a specific form of the Eucken formula [61], which considers only translational and rotational degrees of freedom:

$$k_m = \frac{15}{4} \eta_m ((k_B * N_A) / M_m) (1 + \frac{4}{15}) \quad (16)$$

with $m = \text{CO}_2, \text{CO}$ or O_2 , and η_m and M_m being the corresponding viscosity and molar mass. η_m (in $\text{Pa} \times \text{s}$) is calculated as [62,63]:

$$\eta_m = 2.669e^{-6} \frac{\sqrt{T_g M_m \times 10^3}}{\sigma_m^2 \Omega_D} \quad (17)$$

where σ_m is the characteristic length of the Lennard-Jones potential, and Ω_D is the collision integral [64].

The mixture-averaged diffusion coefficient D_m for the species m is given as:

$$D_m = \frac{1 - w_m}{\sum_{i \neq m} \frac{x_m}{D_{i,m}}} \quad (17)$$

where w_m is the mass fraction of species m . The binary diffusion coefficient $D_{i,m}$ is calculated based on the expression from [64–66]. For the charged particles, the diffusion coefficient is calculated from their mobility, taken from [51] or assumed from similar ions, based on the Einstein's relation. Heat capacity, enthalpy and entropy as function of temperature for each species are taken from the NASA polynomials [67,68]. In the computation of T_g , the heat capacity of molecular species with separate vibrational energy balance equations is subtracted of the corresponding vibrational contributions, as described above. For cluster ions, namely C_2O_2^+ , C_2O_3^+ , C_2O_4^+ , CO_4^+ and CO_4^- , the heat capacity is neglected, because their low concentrations do not affect the computations, while enthalpy and entropy are taken from [69,70] without temperature dependence, with a constant value at ca. 300 K, depending on the source measurement. The uncertainty that this approximation brings to the computations is very small due to the low concentrations of these species and the narrow temperature range of this study. The thermal

conductivity of CO₂ calculated in this way was compared to the thermal conductivity as a function of temperature available in literature and the agreement was within 5 %.

We must point out that, for each of the above balance equations, we have checked that the energy is conserved by summing the time-dependent and heat terms.

3. Results and discussion

The experimental conditions investigated in this study correspond to the single-pulse measurement of Klarenaar *et al.* [10]. The pressure is kept constant at 6.7 mbar and the feed flow rate is 166 sccm. The pulse-on time is 5 ms, with a current of 50 mA. The plasma length and radius are 17 and 1 cm, respectively. Our model represents the first fully self-consistent model describing the single-pulse experiment of Klarenaar *et al.* [10], starting from the experimental current profile as input parameter, without the need to assume a priori electron density or temperature, or E/N. To achieve such degree of self-consistency, our model includes the electrical circuit, the ion kinetics, the electron temperature and the vibrational and gas temperature balance equations, in contrast to the existing models, which use the electron density profile or gas temperature profile as input to the simulations. Moreover, using energy balance equations instead of the STS description of the vibrational kinetics drastically reduces the number of reactions, making this kinetic model suitable for implementation in CFD models.

3.1. Temperature evolutions and comparison with experiments

Figure 1 compares the calculated temporal profiles of the various temperatures with the experimental results.

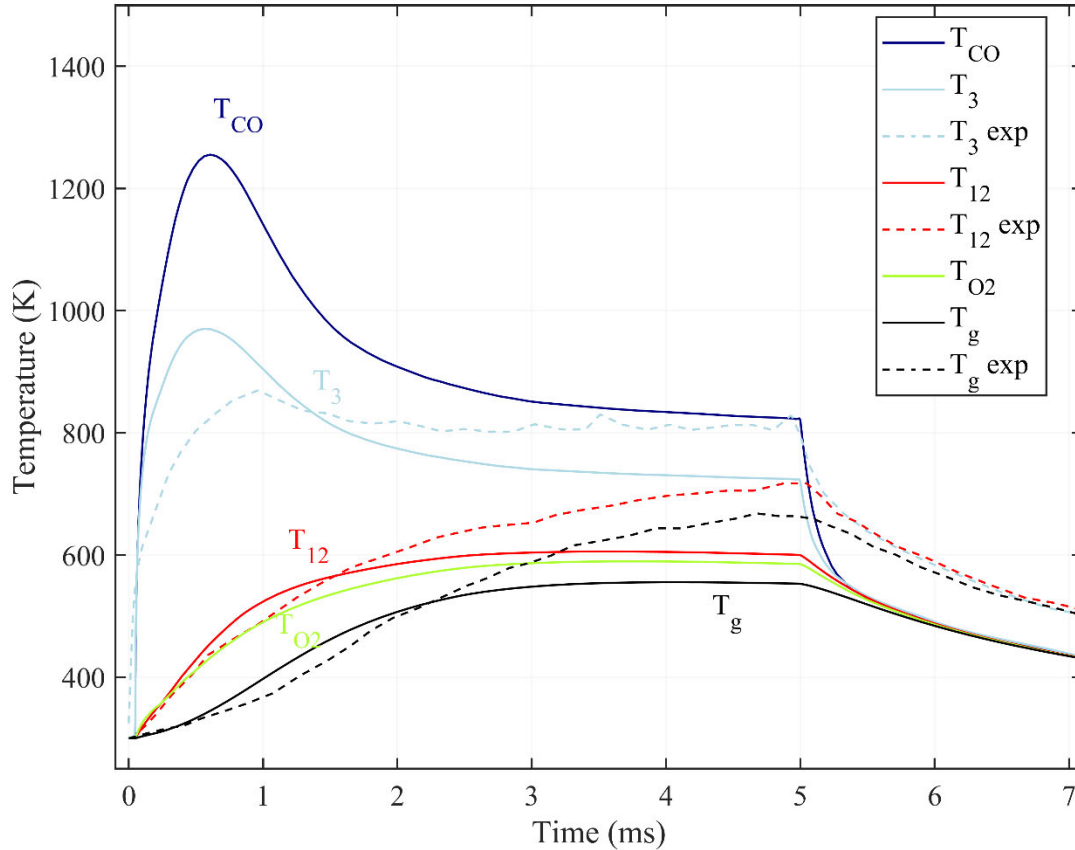


Figure 1. Calculated (solid lines) and experimental (dashed, when available) temperature profiles for the single-pulse experiment of [10].

Overall, we reach satisfactory agreement between calculated and experimental temperature profiles during the first part of the pulse. However, significant deviations arise for the second part of the pulse, especially for T_g and the closely related T_{12} and T_{O_2} profiles. This can be ascribed to the way heat losses to the walls are accounted for in the model. Particularly, eq. (9) in section 2.4 describes heat conduction averaged over the tube radius, with a factor 8 in front of the conduction

term. This is ideal for comparing the computed profiles with radially averaged experimental temperatures. However, Klarenaar *et al.* [10] measured the temperatures at the center of the tube radius; thus, the factor 8 in front of the conduction term (cf. eq. (9) above) has to be replaced by a factor 4, when calculating the gas temperature in the center of the reactor [55]. Figure 2 presents calculated (solid lines) and experimental (dashed, when available) temperature profiles for the single-pulse experiment of [10] using the heat balance equation for the center of the reactor, allowing a more correct comparison with the experiment.

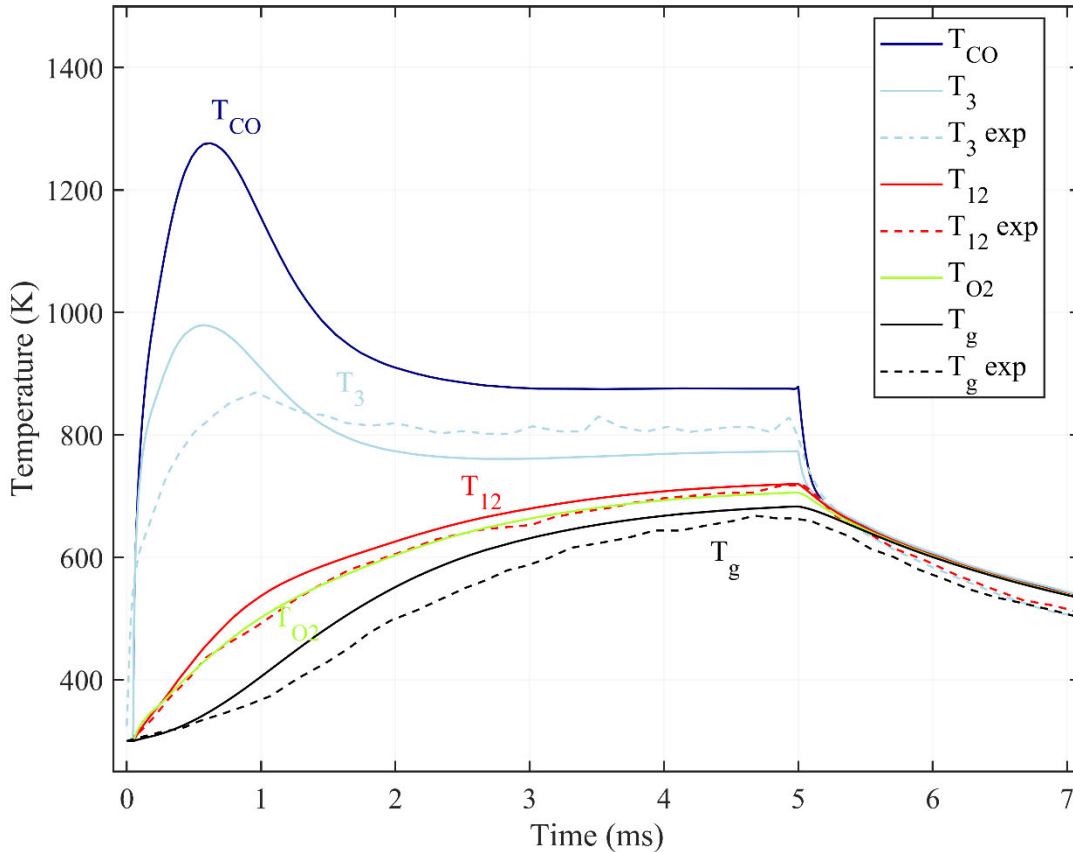


Figure 2. Calculated (solid lines) and experimental (dashed, when available) temperature profiles for the single-pulse experiment of [10] using the heat balance equation for the center of the reactor, needed to compare with the experiment.

Compared to Figure 1, Figure 2 shows improved agreement between the computed and experimental temperature profiles, especially in the second part of the pulse for T_{12} and T_g , which were earlier strongly underestimated. The difference between Figure 1 and 2 is a consequence of the strong dependence of T_{12} and T_g on the conduction term, as the corresponding degrees of freedom have a high heat capacity and transfer a substantial amount of energy to the walls through conduction. This underscores the critical importance of accurately understanding the shape of the temperature profile when applying the energy approach in modeling non-equilibrium conditions.

By examining the temporal profiles, we observe that T_{CO} closely follows the profile of T_3 and remains elevated throughout the entire duration of the pulse. Due to the low degree of dissociation and vibrational non-equilibrium, we do not account for dissociation processes occurring through high vibrational levels of the asymmetric stretching mode (T_3), known as the “ladder-climbing mechanism” [8,24]. Nevertheless, our results indicate that, under these conditions, the excitation of T_{CO} is likely to promote $CO + O$ recombination back to CO_2 . This effect was briefly mentioned by Rusanov *et. al.* [71], who estimated that when $T_{CO} \cong T_3$, the forward and reverse rate of dissociation equilibrate, reducing the overall energy efficiency by 30%. In our study, $T_{CO} > T_3$, suggesting that the recombination might be favored over dissociation. Indeed, the vibrationally enhanced reverse reaction is often overlooked in literature due to the additional complexity it introduces into the system. Our results highlight the necessity of including the vibrational energy balance of the products, along with that of the feed components, to correctly describe the dynamics of the system.

In the next section, we delve deeper into the individual energy balance equations to reconstruct the heating dynamics. From now on, only the results for the centerline temperatures, with a factor 4 in the conduction terms, are presented.

3.2. Heating dynamics of the gas and vibrational modes

Given the reasonable agreement for the temperature profiles, we can now examine the gas heating dynamics by looking at the individual energy balances. The energy balance of T_3 is presented in Figure 3.

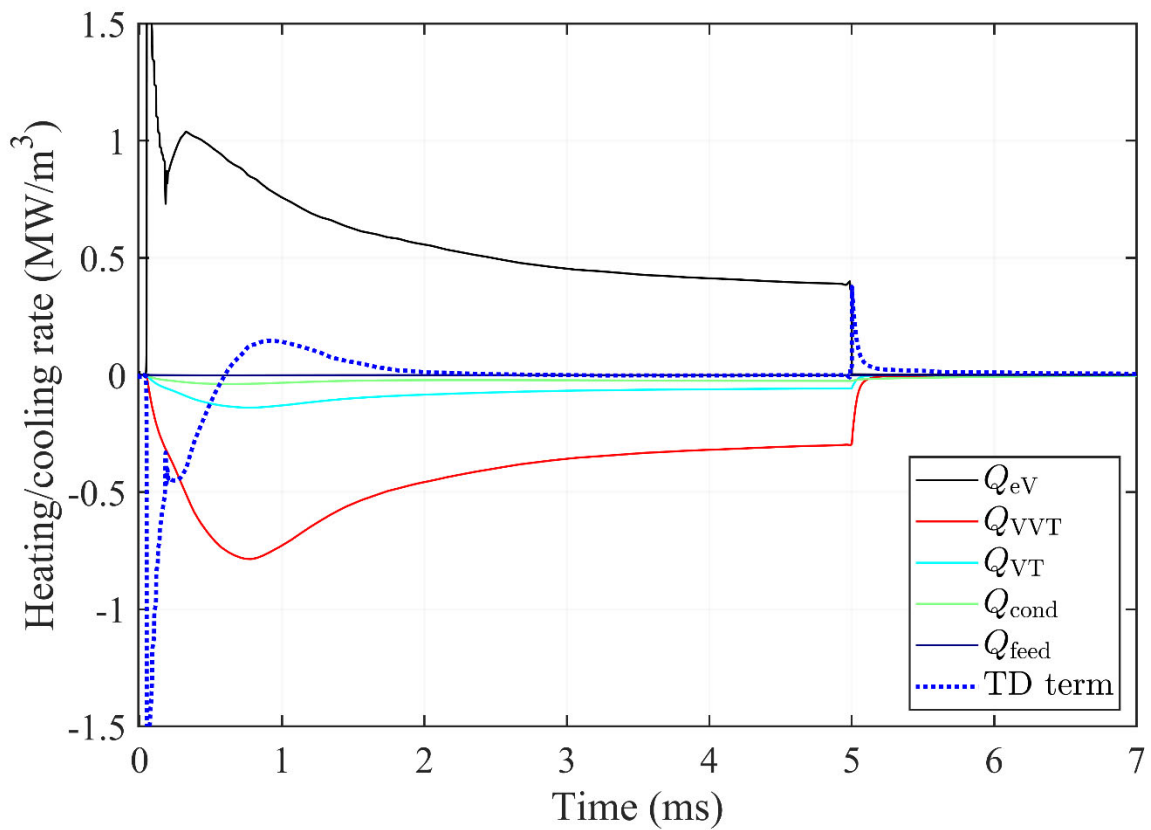


Figure 3. Contributions to the energy balance of T_3 , see eq. (11), including the time-dependent (TD) term.

Figure 3 indicates that T_3 is exclusively heated by electron-impact excitation (Q_{eV}), whereas the dominant cooling mechanism is V-V-T relaxation to T_{12} . V-T relaxation and heat conduction to

the walls play a minor role. Due to the low heat capacity, T_3 is significantly higher than T_{12} (cf. Figure 2 above). The lower heat capacity also implies that the energy conduction towards the walls is reduced, assuming a parabolic dependence of the vibrational temperature profile. The same analysis is performed for T_{12} in Figure 4.

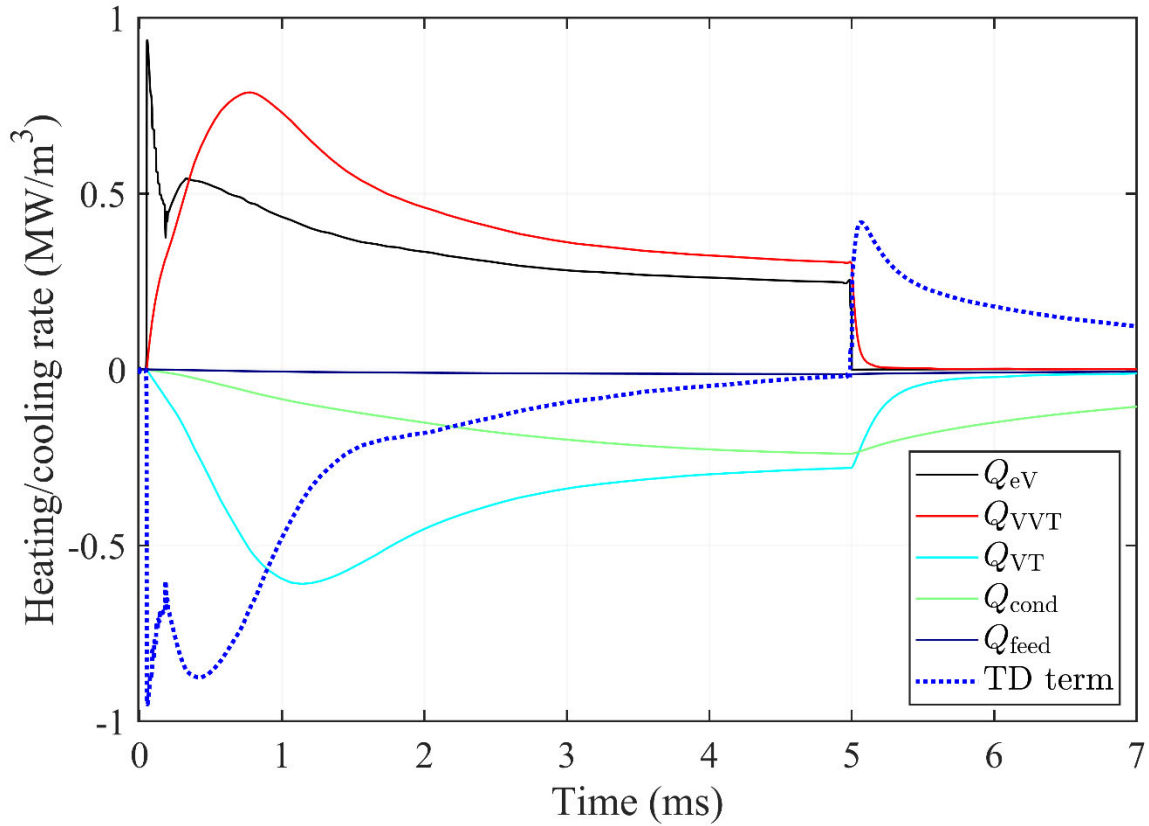


Figure 4. Contributions to the energy balance of T_{12} , see eq. (8), including the time-dependent (TD) term.

The dominant cooling mechanism for T_3 (i.e., Q_{VVT}) is an important heating channel for T_{12} , in line with the modelling results of Biondo *et al.* [36], who showed that V-V-T relaxation is responsible for coupling the asymmetric and symmetric levels of CO_2 . Equally important is

electron-impact excitation, which constitutes approximately half of the heating rate for T_{12} . V-T relaxation is the primary cooling pathway, as also reported in previous studies (*e.g.*, [32,36]). However, heat conduction to the walls becomes as important in the second part of the pulse, and is the dominant cooling mechanism in the afterglow. This is consistent with what was described by Thomson *et al.* [60], indicating that the vibrational component of the thermal conductivity is responsible for nearly 30% of the total energy flux in CO₂. Thus, the use of the energy approach requires a careful description of the vibrational thermal conductivity in the energy balance equations.

The fact that the rates of V-T relaxation and heat conduction to the walls are comparable is a strikingly different result from previous modelling work, due to the distinct approach used here. Specifically, in many state-to-state modelling studies, such as those by Vermeiren and Bogaerts [72], Silva *et al.* [32], and follow-up works, the energy balance equation for T_g includes vibrational contributions to the heat capacity and thermal conductivity, assuming $T_{\text{vib}} = T_g$. The non-equilibrium vibrational contributions are thus either neglected or treated as wall deactivation [32]. In contrast, the energy approach allows for a more accurate description of the heating dynamics compared to these implementations of the state-to-state approach. However, a state-to-state approach can achieve a similar level of accuracy if only translational and rotational contributions are included in the T_g balance equation, as demonstrated by Nagnibeda and Kustova [73]. Thus, this difference lies not in the state-to-state approach itself, but in the proper treatment of the approximations made when applying it.

The energy balance for T_{CO} and T_{O_2} are not shown because of the very low dissociation degree (ca. 0.4%). Thus, the last energy balance to examine is that of T_g , which is shown in Figure 5.

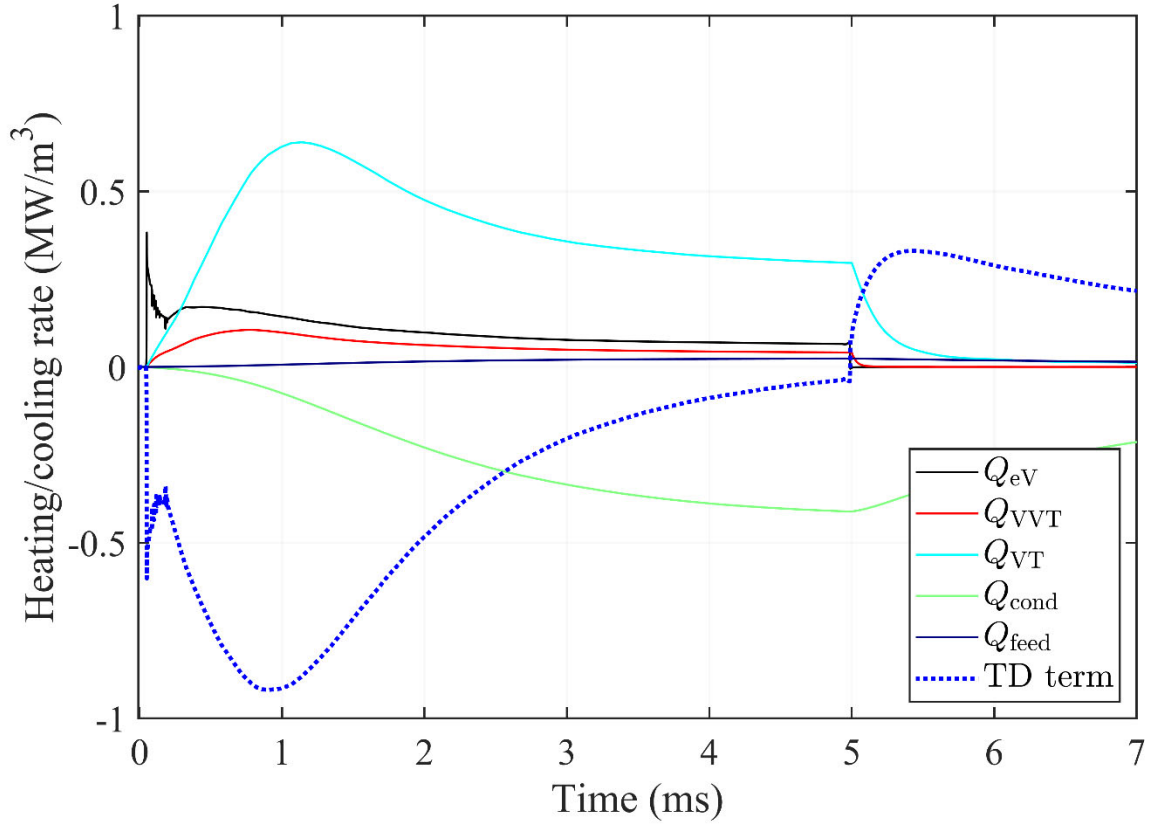


Figure 5. Contributions to the energy balance of T_g , see eq. (14), including the time-dependent (TD) term.

Figure 5 indicates that V-T relaxation is an important pathway of gas heating, becoming the dominant mechanism in the afterglow, but it is not sufficient to describe the overall heating dynamics. Indeed, fast gas heating from reactions (Q_g), especially relaxation of electronic states, is responsible for the elevation of T_g during the first millisecond in the pulse, triggering V-T relaxation as a second heating mechanism. The electronic states contributing the most to fast gas heating are $\text{CO}_2(e_1)$, $\text{CO}_2(e_2)$ and $\text{CO}(a^3\Pi)$. The rest of the electronic states have minimal contributions to the heating dynamics. Despite this, we believe that their inclusion is important in view of extending the validity of this model over a wider range of experimental conditions in the

future. These findings agree well with the observations of Biondo *et al.* [36], who showed that an E/N of more than 90 Td is needed to sustain the discharge, triggering electronic excitation and relaxation, and to achieve a good agreement with measured T_g . Nevertheless, Biondo *et al.* [36] were not able to perform a self-consistent calculation of the electron kinetics and E/N, and had to rely on a constant, estimated E/N of 94 Td for their simulations.

In our study, we go beyond the foundation laid by [36], by incorporating the electrical circuit in our model, with a current source of 50 mA as given by the experimental benchmark [10]. The corresponding calculation results are presented in the next section.

3.3. Electrical characterization: E/N, electrical current and T_e

As we include the electrical circuit in our model, we are able to self-consistently calculate E/N, T_e and current profiles, as shown in Figure 6.

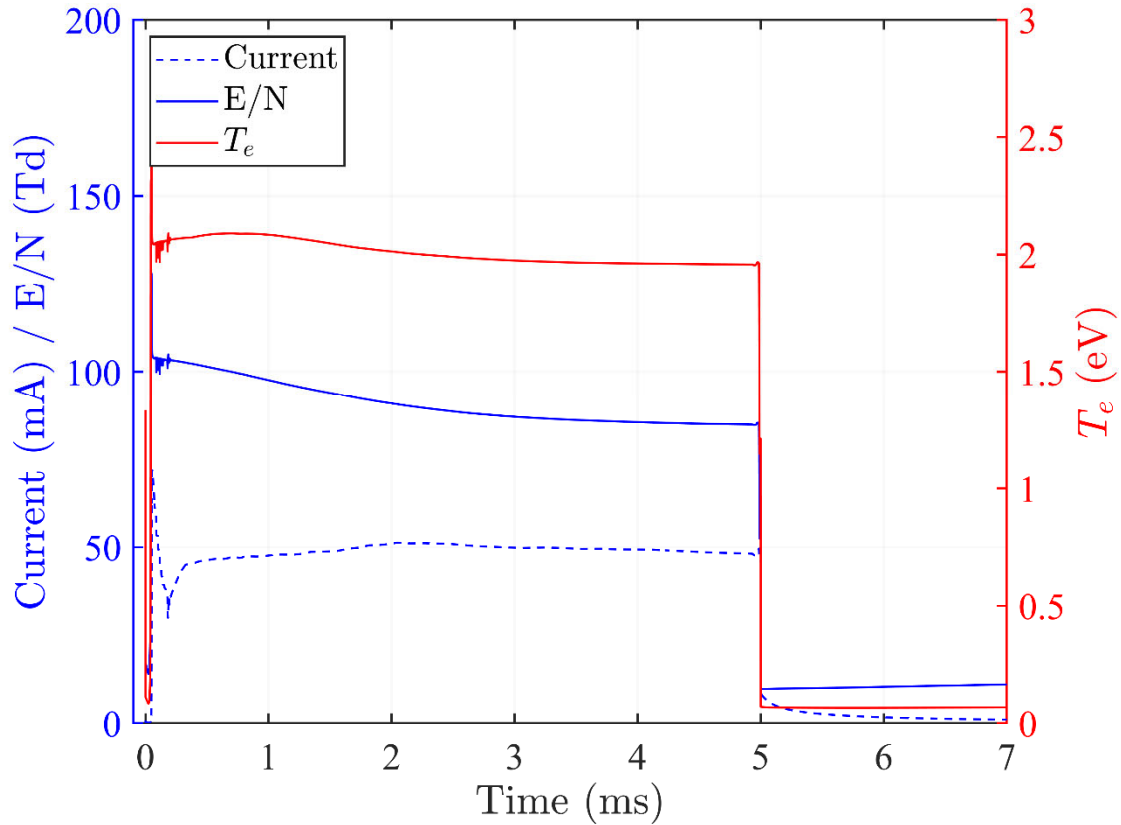


Figure 6. Current, reduced electric field (E/N) and electron temperature (T_e) calculated by our model for the single-pulse experiment of [10].

We can see that in the beginning of the pulse, where the electron density is low and the plasma resistivity high, the reduced electric field has a value of nearly 120 Td. As the electron density and the plasma conductivity are increasing, the electric field needed to sustain the discharge is reduced. As a result, the value of E/N gradually drops to 94 Td towards the end of the pulse. Figure 6 confirms that the discharge is sustained at $E/N > 90$ Td, in line with the findings of [36], corresponding to $T_e > 2$ eV. To achieve this, the inclusion of ambipolar diffusion of positive ions and electrons to the reactor walls is essential. Without it, the computed plasma parameters become unreasonable shortly after the breakdown, making the simulations challenging to solve.

3.4. Ion kinetics

In order to calculate the plasma properties of Figure 6 in a self-consistent manner, our model includes a detailed description of the ion kinetics. This is necessary to predict the correct electron density, which is very similar to the one estimated in [31], although achieved at a higher E/N.

Figure 7 shows the time evolution of the number densities of the main ions and the electrons.

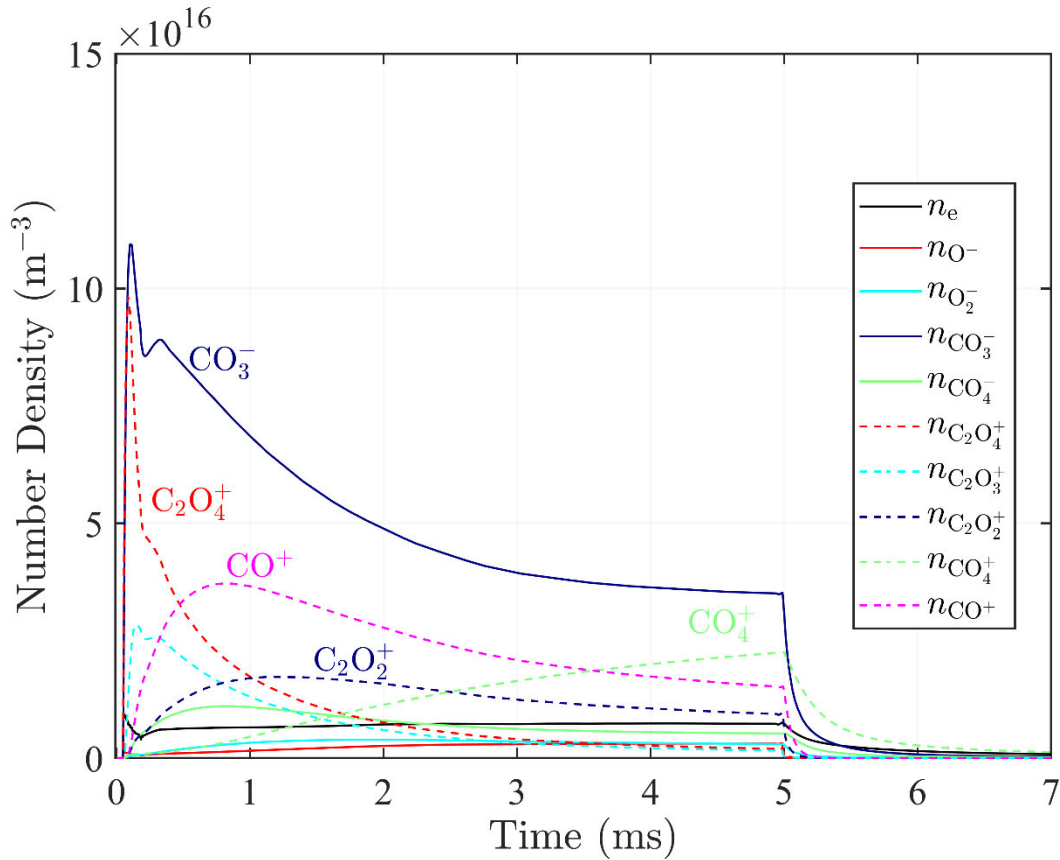


Figure 7. Time evolution of the electron and dominant ion number densities.

Including a complete set of ion kinetics reveals that the dominant negative ion during the pulse is CO_3^- , which has a much higher density than the electrons. It results from dissociative electron

attachment to CO₂ forming O⁻, and subsequent recombination of O⁻ with CO₂ to form the stable CO₃⁻ ion [74]. In fact, electron detachment from this ion has a high energy threshold [75], and thus the ion is only efficiently lost via ion-ion recombination and collisional detachment with O atoms and CO. Despite its importance, the corresponding chemistry is not well understood and is often omitted in CO₂ plasma modeling. For instance, Naidis and Babaeva [76] did not include CO₃⁻ in their work, when modelling similar experiments (same pressure but lower mass flow rate, with higher pulse repetition rate) [10]. Their conclusion was that CO₃⁻ is not formed, because O⁻ is effectively quenched through collisions with CO. However, our model shows that quenching upon collision with CO is not effective enough to remove the ion, due to the low dissociation degree in the single-pulse experiment. The second important negative ion is CO₄⁻, originating from a clustering reaction between O₂⁻ and CO₂ [47], but its density is much lower than for CO₃⁻, and comparable to or even slightly higher than n_e . As a result of the high negative ion densities, the electrons are lost primarily by attachment reactions, rather through ambipolar diffusion. This effect increases the reduced electric field until a sufficient amount of CO is produced.

The dominant positive ions are a result of clustering reactions as well, and subsequent charge transfer reactions. Initially, C₂O₄⁺ is formed from CO₂⁺ + 2CO₂ → C₂O₄⁺ + CO₂ [77]. Then, C₂O₄⁺ reacts with CO, originating from the dissociation of CO₂, to produce C₂O₃⁺ and CO₂. As the O₂ concentration builds up during the pulse, C₂O₄⁺ is converted to CO₄⁺ through C₂O₄⁺ + O₂ + CO₂ → CO₄⁺ + 2CO₂ [78]. Thus, CO₄⁺ becomes the dominant positive ion in the second part of the pulse and in the afterglow.

Conclusions

Fully self-consistent modeling of CO₂ plasmas can unlock the potential of plasma-based CO₂ conversion for the electrification of fossil fuel-based sectors, such as the chemical industry. However, the road ahead for fully self-consistent (and predictive) models is still very long, due to the multitude of physical phenomena that need to be thoroughly considered and captured, *e.g.*, fluid dynamics, heat transfer, chemical kinetics, and the interplay between them.

In this study, we focus on the kinetics underlying vibrational and gas heating in a pulsed CO₂ glow discharge, operated at low pressure. This type of discharge represents the ideal case to validate a kinetic scheme due to the homogeneity of the plasma. Moreover, pulsing enables to capture the transient behavior of the electron kinetics and the relaxation of excited species, and compare them with global computations.

Starting from the foundations laid by previous modelling efforts, we construct a fully self-consistent kinetic model based on an energy approach, with separate energy balance equations for the vibrational temperatures of CO₂ (both asymmetric and symmetric modes), CO and O₂, the gas temperature, and the electron temperature. The latter is a particularly innovative aspect, introduced for the first time by our model. In fact, the models published so far have failed to include a fully self-consistent description of the electron kinetics using the experimental current as an input parameter. We were able to achieve this by coupling the plasma to an electrical circuit and resolving the extensive ion chemistry, which is rarely considered in recent literature. This is possible by the drastic reduction in the number of reactions within the model, achieved by replacing the detailed, state-to-state vibrational kinetics with the energy approach. Therefore, these represent additional innovative features of our model.

Comparison with the temporal evolution of the measured temperature profiles shows satisfactory agreement, indicating that our model includes all the relevant kinetics, at least for the single-pulse

experiment, where the dissociation degree is limited and all dissociation products are evacuated before the subsequent pulse. Therefore, we can consider our model to be validated for CO₂ discharges at low pressure and low excitation, for which the dissociation degree of CO₂ is smaller than 1%. Hence, the simulation outcome can be used to infer the underlying dynamics, confirming the importance of vibrational-vibrational relaxation, coupling the asymmetric and symmetric levels of CO₂. Moreover, our study highlights the important role of vibrational energy transfer to the walls for an accurate description of the gas heating.

Furthermore, our study reveals the importance of CO₃⁻ in describing the dynamics of the system. Due to the low dissociation degree, CO₃⁻ is efficiently produced, which results in an increase of the reduced electric field, needed to sustain the specified current. The CO₃⁻ density is an order of magnitude higher than the electron density, resulting in significant losses due to attachment reactions. The detailed description of the formation and destruction of positive and negative ions, as well as their interactions with electrons and neutrals, allows us to self-consistently simulate the behavior of the reduced electric field, eliminating significant assumptions previously necessary for modelling transient discharges.

Notwithstanding the successful results of this study, our model is still limited to conditions that are far from appealing for industrial application, namely atmospheric (or higher) pressure and high CO₂ conversion. The next step towards such conditions is to compare our model with experiments where the effects of dissociation products are significant, such as the multi-pulse experiment by Damen *et al* [17]. This experiment presents conditions with more prominent gas heating and higher fractions of species with high thermal conductivity (e.g., O and O₂). In doing so, we anticipate that the model will require a more detailed description of radial heat losses to the reactor walls. Additionally, the model will need to include the dependence of chemical reactions on all the six

temperatures for more accurate description of dissociation and recombination dynamics, as previously presented by Kosareva *et al.* [54]. For these reasons, incorporating the validated chemical kinetics from this study into a 1D radial model will be a necessary step towards self-consistent CFD modeling of CO₂ discharges, for reactor optimization and design.

Conflict of interest

There are no conflicts of interest to declare.

Acknowledgments

We gratefully acknowledge financial support by the Fund for Scientific Research (FWO; grant ID 1205424N), the European Research Council (ERC) under the European Union's Horizon 2020 research and innovation programme (grant agreement no. 810182; SCOPE ERC Synergy project), and the VLAIO-Catalisti ICON project "BluePlasma" (grant ID HBC.2022.0445).

Data availability statement

The data that supports the findings of this study is available upon reasonable request from the authors.

Appendix

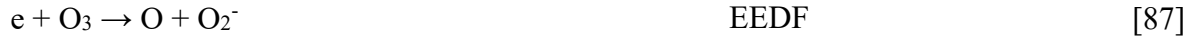
A1. Chemistry set

The electron-impact processes, described by energy-dependent cross sections and the EEDF, are taken from specific databases within the LxCat database, as detailed in the reference column of Table A1. The cross sections for direct electron-impact dissociation of CO₂ have been modified compared to the original set, following the adjustments in Biondo *et al.* [36]. The consistency of these updated cross sections with the swarm parameters was verified in the same study. For all other reactions, rate coefficients and corresponding references are given in Table A1.

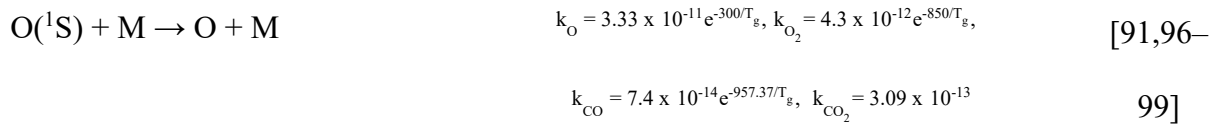
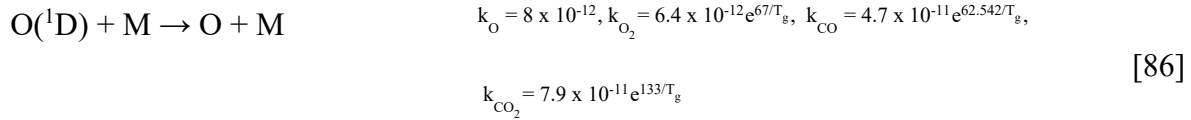
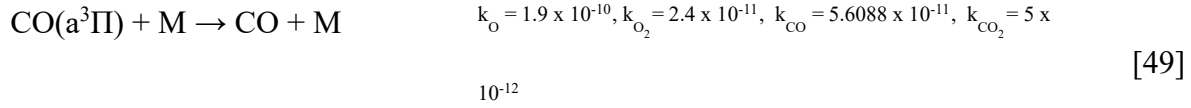
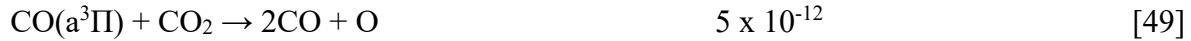
Table A1. Chemistry set used in this work. Rate coefficients are in s⁻¹, cm³/s or cm⁶/s, for radiative decay, two-body and three-body reactions, respectively, while T_e and T_g are both expressed in K. N_n represents the total neutral density in cm⁻³, while M is a colliding partner and k_M the corresponding rate coefficient. Most of the electron-impact processes are described by energy-dependent cross sections and the EEDF, as indicated in the table.

Reaction	Rate expression	Ref.
Electron-impact processes		
$e + \text{CO}_2 \rightarrow e + \text{CO}_2$	EEDF	[79]
$e + \text{CO}_2 \rightarrow e + e + \text{CO}_2^+$	EEDF	[79]
$e + \text{CO}_2 \leftrightarrow e + \text{CO}_2(v_1v_2v_3)^a$	EEDF	[79]
$e + \text{CO}_2 \leftrightarrow e + \text{CO}_2(e1,e2)$	EEDF	[36,79]
$e + \text{CO}_2 \rightarrow e + \text{CO} + \text{O}(^1\text{D})$	EEDF	[36,80]
$e + \text{CO}_2 \rightarrow e + \text{CO}(a^3\Pi) + \text{O}$	EEDF	[36,80]
$e + \text{CO}_2 \rightarrow \text{CO} + \text{O}^-$	EEDF	[79]
$e + \text{CO} \rightarrow e + \text{CO}$	EEDF	[81]
$e + \text{CO} \rightarrow e + e + \text{CO}^+$	EEDF	[81]

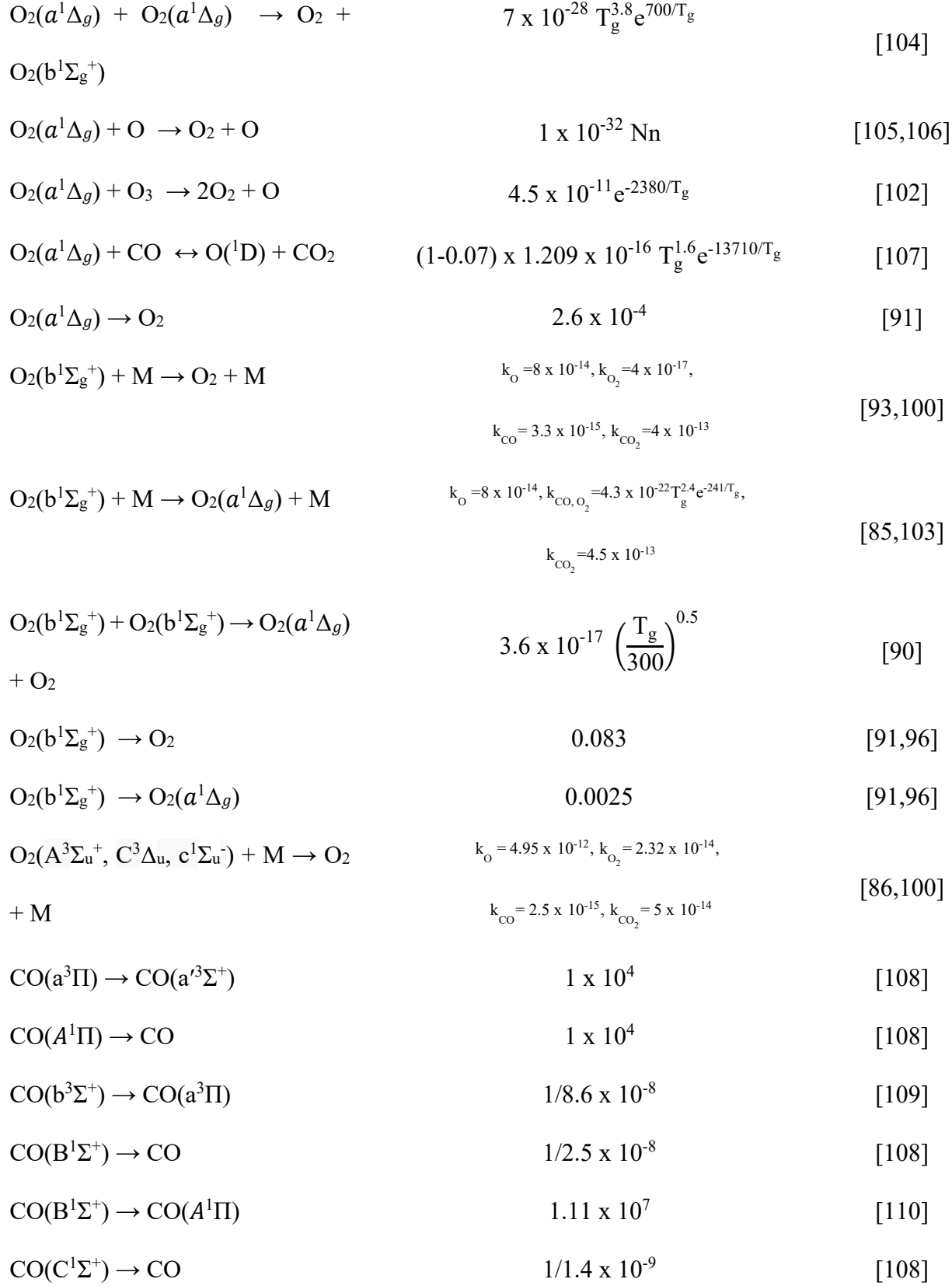
$e + CO \leftrightarrow e + CO(v)$	EEDF	[81]
$e + CO \leftrightarrow e + CO(a^3\Pi, a'^3\Sigma^+, A^1\Pi,$	EEDF	[81]
$b^3\Sigma^+, B^1\Sigma^+, C^1\Sigma^+, E^1\Sigma^+)$		
$e + CO \rightarrow e + C + O$	EEDF	[81]
$e + CO \rightarrow C + O^-$	EEDF	[81]
$e + O_2 \rightarrow e + O_2$	EEDF	[82,83]
$e + O_2 \rightarrow e + e + O_2^+$	EEDF	[82,83]
$e + O_2 \leftrightarrow e + O_2(v)$	EEDF	[82,83]
$e + O_2 \leftrightarrow e + O_2(a^1\Delta_g, b^1\Sigma_g^+,$	EEDF	[82,83]
$A^3\Sigma_u^+, C^3\Delta_u, c^1\Sigma_u^-)$		
$e + O_2 \rightarrow e + O + O$	EEDF	[82,83]
$e + O_2 \rightarrow e + O + O(^1D)$	EEDF	[82,83]
$e + O_2 \rightarrow O + O^-$	EEDF	[82,83]
$e + O_2 + M \rightarrow O_2^- + M$	$k_{CO_2,CO} = 3.3 \times 10^{-30}, k_O = 1 \times 10^{-31},$	[84–86]
	$k_{O_2} = 1.4 \times 10^{-29} \times 300/T_e \times e^{-\frac{600}{T_g}} \times e^{-\left(\frac{700(T_e - T_g)}{T_e T_g}\right)}$	
$e + O \rightarrow e + O$	EEDF	[87]
$e + O \rightarrow e + e + O^+$	EEDF	[87]
$e + O \rightarrow O^-$	$k_M = 1 \times 10^{-31} \times N_n$	[85]
$e + O \leftrightarrow e + O(^1D, ^1S)$	EEDF	[87]
$e + C \rightarrow e + C$	EEDF	[88]
$e + O_3 \rightarrow e + O_3$	EEDF	[87]
$e + O_3 \rightarrow e + e + O_3^+$	EEDF	[87]

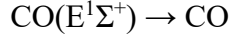


Electronic relaxation



$O(^1S) + M \rightarrow O(^1D) + M$	$k_{O} = 5 \times 10^{-11} e^{-301/T_g}, k_{O_2} = 1.333 \times 10^{-12} e^{-850/T_g},$	[86,97,10
	$k_{CO} = 9.4 \times 10^{-14}, k_{CO_2} = 2.394 \times 10^{-13}$	0,101]
$O(^1S) + O_2 \rightarrow O + O_2(a^1\Delta_g)$	$1.5 \times 10^{-12} e^{-850/T_g}$	[86]
$O(^1S) + O_2 \rightarrow O + O_2(b^1\Sigma_g^+)$	$7.3 \times 10^{-13} e^{-850/T_g}$	[86]
$O(^1S) + O_2 \rightarrow O + O_2(A^3\Sigma_u^+,$ $C^3\Delta_u, c^1\Sigma_u^-)$	$2.967 \times 10^{-12} e^{-850/T_g}$	[86]
$O(^1S) + O_2(a^1\Delta_g) \rightarrow O + O_2$	1×10^{-10}	[90]
$O(^1S) + O_2(a^1\Delta_g) \rightarrow O +$ $O_2(b^1\Sigma_g^+)$	1.3×10^{-10}	[90]
$O(^1S) + O_2(a^1\Delta_g) \rightarrow O(^1D) + O_2$	3.6×10^{-11}	[90]
$O(^1S) + O_2(a^1\Delta_g) \rightarrow 3O$	3.23×10^{-11}	[86]
$O(^1S) + O_2(a^1\Delta_g) \rightarrow O +$ $O_2(A^3\Sigma_u^+, C^3\Delta_u, c^1\Sigma_u^-)$	7.905×10^{-11}	[86]
$O(^1S) + O_2(a^1\Delta_g) \rightarrow O(^1D) +$ $O_2(a^1\Delta_g)$	1.7×10^{-12}	[86]
$O(^1S) + O_2(a^1\Delta_g) \rightarrow O(^1D) +$ $O_2(b^1\Sigma_g^+)$	2.89×10^{-11}	[86]
$O(^1S) \rightarrow O(^1D)$	1.3	[91]
$O(^1S) \rightarrow O$	0.078	[91]
$O_2(a^1\Delta_g) + M \rightarrow O_2 + M$	$k_{O} = 7 \times 10^{-16}, k_{O_2} = 2.2 \times 10^{-18} \left(\frac{1}{300}\right)^{0.8},$	[86,102,1
	$k_{CO,CO_2} = 3.8 \times 10^{-18} e^{-205/T_g}$	03]

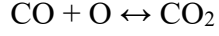




$$k_{\text{O}} = 1.9 \times 10^{-10}, k_{\text{O}_2} = 2.4 \times 10^{-11}, k_{\text{CO}} = 5.6088 \times 10^{-11}, k_{\text{CO}_2} = 5 \times 10^{-12}$$

This work

Neutral reactions

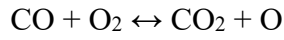


$$3 \times 10^{-14} \times e^{-\frac{1219}{T_g}} / \left(1 + \frac{3 \times 10^{-14} \times e^{-\frac{1219}{T_g}}}{10^{-32} \times e^{-\frac{1500}{T_g}} \times c_{\text{eff}}[M]}\right),$$

[111]

with $c_{\text{eff}} = 3.5, 6, 1.5, 1$, for $M = \text{CO}_2, \text{O}_2,$

CO , and C and O , respectively



$$4.15 \times 10^{-12} \times e^{-24054/T_g}$$

[111]



$$4 \times 10^{-25}$$

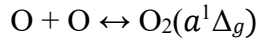
[91]



$$2.4 \times 10^{-21} + 0.5 \times 3.8 \times 10^{-30} T_g^{-1} \times e^{-170/T_g} \times (\text{Nn} -$$

[91,102]

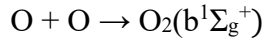
$$n_{\text{O}} - n_{\text{O}_2(a^1\Delta_g)})$$



$$0.33 \times 3.8 \times 10^{-30} T_g^{-1} \times e^{-170/T_g} \times (\text{Nn} - n_{\text{O}} -$$

[102]

$$n_{\text{O}_2(a^1\Delta_g)})$$



$$0.17 \times 3.8 \times 10^{-30} T_g^{-1} \times e^{-170/T_g} \times \text{Nn}$$

[102]



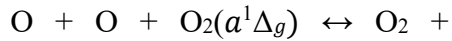
$$1.2 \times 10^{-34} \times \text{Nn}$$

[86]



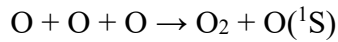
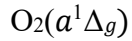
$$2.5 \times 10^{-31} T_g^{-0.63}$$

[104]



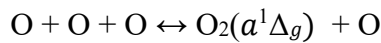
$$7.4 \times 10^{-33}$$

[90]



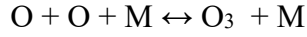
$$1.4 \times 10^{-30} \times e^{-650/T_g}$$

[91]



$$6.93 \times 10^{-35} T_g^{-0.63}$$

[90]



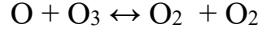
$$k_{\text{CO}_2, \text{CO}} = 1.81 \times 10^{-33} \left(\frac{T_g}{300} \right)^{-1.2},$$

[86,102,1

$$k_{\text{O}_2} = 6.9 \times 10^{-34} \left(\frac{T_g}{300} \right)^{-1.25},$$

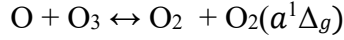
04]

$$k_{\text{O}} = 2.1 \times 10^{-34} \times e^{245/T_g}$$



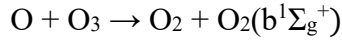
$$0.5 \times 1.8 \times 10^{-11} \times e^{-2300/T_g}$$

[86]



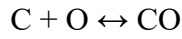
$$0.33 \times 1.8 \times 10^{-11} \times e^{-2300/T_g}$$

[86]



$$0.17 \times 1.8 \times 10^{-11} \times e^{-2300/T_g}$$

[86]



$$2.14 \times 10^{-29} \left(\frac{T_g}{300} \right)^{-3.08} e^{-2114/T_g} \times \text{Nn}$$

[111]



$$9.63 \times 10^{-11} \times e^{-290/T_g}$$

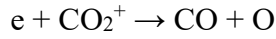
[111]



$$1 \times 10^{-15}$$

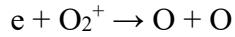
[111]

Electron-ion recombination



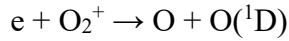
$$4.2 \times 10^{-7} \left(\frac{T_e}{300} \right)^{-0.75}$$

[112]



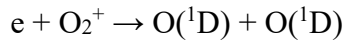
$$0.32 \times 1.95 \times 10^{-7} \left(\frac{T_e}{300} \right)^{-0.7}$$

[113,114]



$$0.43 \times 1.95 \times 10^{-7} \left(\frac{T_e}{300} \right)^{-0.7}$$

[113,114]



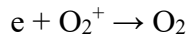
$$0.2 \times 1.95 \times 10^{-7} \left(\frac{T_e}{300} \right)^{-0.7}$$

[113,114]



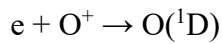
$$0.04 \times 1.95 \times 10^{-7} \left(\frac{T_e}{300} \right)^{-0.7}$$

[113,114]



$$6 \times 10^{-27} \left(\frac{T_e}{300} \right)^{-1.5} \times \text{Nn}$$

[85]



$$5 \times 10^{-13} T_e^{-0.5}$$

[90]

$$e + O^+ \rightarrow O \quad 6 \times 10^{-27} \left(\frac{T_e}{300}\right)^{-1.5} \times Nn \quad [85]$$

$$e + CO^+ \rightarrow C + O \quad 2.75 \times 10^{-7} \left(\frac{T_e}{300}\right)^{-0.55} \quad [115]$$

$$e + CO_4^+ \rightarrow CO_2 + O_2 \quad 1 \times 10^{-6} \left(\frac{T_e}{300}\right)^{-0.5} \quad [116]$$

$$e + C_2O_2^+ \rightarrow CO + CO \quad 1.3 \times 10^{-6} \left(\frac{T_e}{300}\right)^{-0.34} \quad [117]$$

$$e + C_2O_3^+ \rightarrow CO_2 + CO \quad 5.4 \times 10^{-8} \left(\frac{T_e}{300}\right)^{-0.7} \quad [46]$$

$$e + C_2O_4^+ \rightarrow CO_2 + CO_2 \quad 2 \times 10^{-5} T_e^{-0.5} T_g^{-1} \quad [46]$$

$$e + O_3^+ \rightarrow O_2 + O \quad 1.95 \times 10^{-7} \left(\frac{T_e}{300}\right)^{-0.7} \quad \text{This study}$$

$$e + O_4^+ \rightarrow O_2 + O_2 \quad 1.4 \times 10^{-6} \left(\frac{T_e}{300}\right)^{-0.5} \quad [85]$$

$$e + A^+ \rightarrow A \quad 5.5 \times 10^{-25} \left(\frac{T_g}{T_e}\right)^{3/2} \times Nn \quad [118,119]$$

A = C, CO, CO₂, O₃

$$e + AB^+ \rightarrow A + B \quad 5.5 \times 10^{-25} \left(\frac{T_g}{T_e}\right)^{3/2} \times Nn \quad [118,119]$$

AB = C₂O₂, C₂O₃, C₂O₄, CO₄, O₄

$$e + e + A^+ \rightarrow e + A \quad 1 \times 10^{-19} \left(\frac{300}{T_e}\right)^{4.5} \quad [85,120]$$

A = O, C, CO, O₂, CO₂, O₃

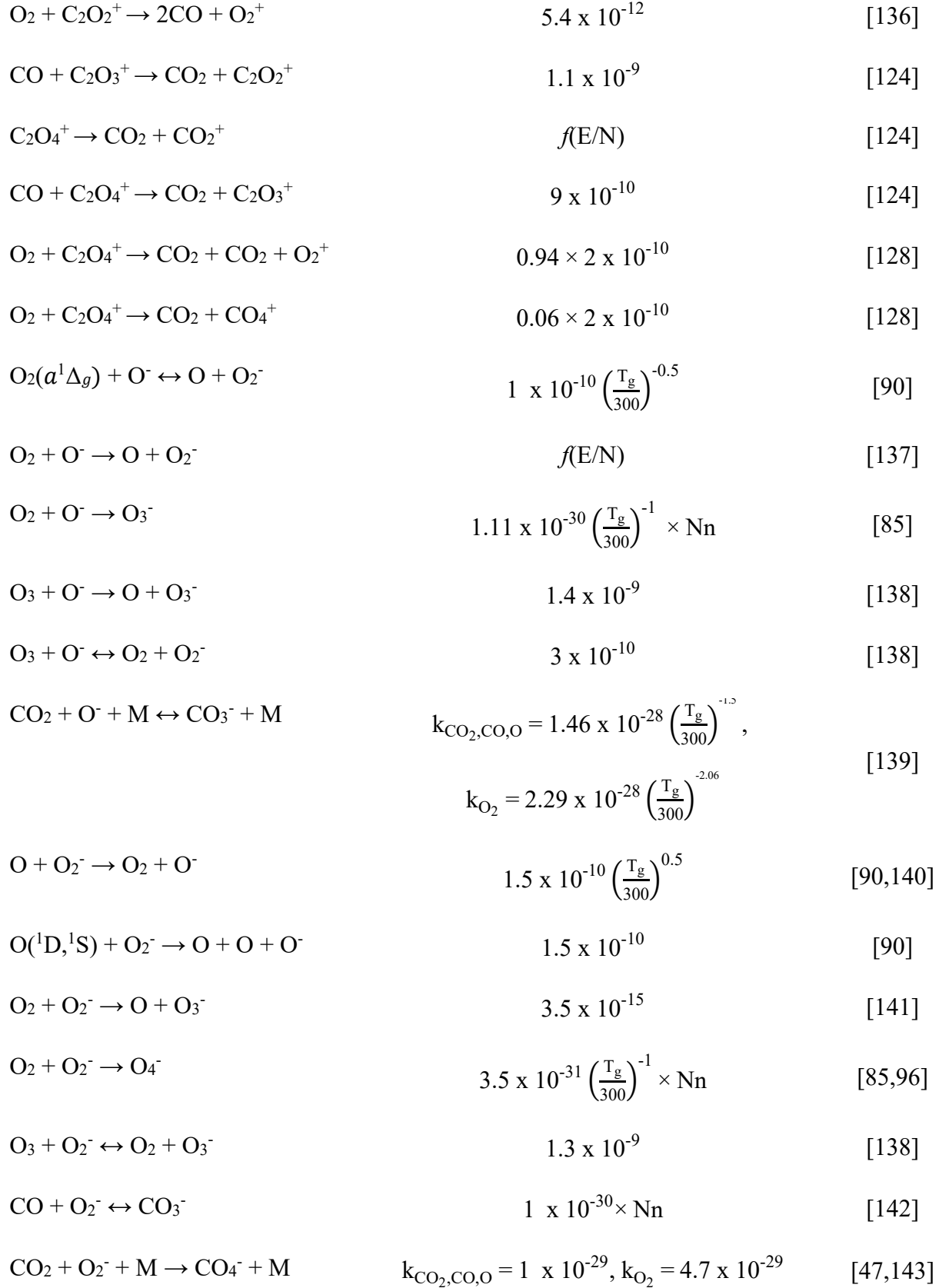
$$e + e + AB^+ \rightarrow e + A + B \quad 1 \times 10^{-19} \left(\frac{300}{T_e}\right)^{4.5} \quad [85,120]$$

AB = C₂O₂, C₂O₃, C₂O₄, CO₄, O₄

Ion-neutral reactions

$$O + CO_2^+ \leftrightarrow CO + O_2^+ \quad 1.64 \times 10^{-10} \quad [121]$$

$O + CO_2^+ \leftrightarrow CO_2 + O^+$	9.63×10^{-11}	[121]
$O_2 + CO_2^+ \leftrightarrow CO_2 + O_2^+$	5.5×10^{-11}	[122,123]
$CO_2 + CO_2^+ \rightarrow C_2O_4^+$	$7 \times 10^{-28} \times N_n$	[124]
$C + O_2^+ \leftrightarrow O + CO^+$	5.2×10^{-11}	[125]
$C + O_2^+ \leftrightarrow O_2 + C^+$	5.2×10^{-11}	[125]
$O_2 + O_2^+ \rightarrow O_4^+$	$2.4 \times 10^{-30} \left(\frac{T_g}{300}\right)^{-3.2} \times N_n$	[126]
$CO_2 + O_2^+ + M \rightarrow CO_4^+ + M$	$k_{CO,O,O_2} = 2.3 \times 10^{-29}, k_{CO_2} = 1.2 \times 10^{-29}$	[126–128]
$CO_2 + CO^+ \leftrightarrow CO + CO_2^+$	1×10^{-15}	[129]
$O_2 + CO^+ \leftrightarrow CO + O_2^+$	$1.5 \times 10^{-10} \left(\frac{T_g}{300}\right)^{-1.1}$	[123,130]
$O + CO^+ \leftrightarrow CO + O^+$	1.4×10^{-10}	[131]
$C + CO^+ \leftrightarrow CO + C^+$	1.4×10^{-10}	[125]
$CO + CO^+ \rightarrow C_2O_2^+$	$1.48 \times 10^{-28} \times N_n$	[132,133]
$O + O^+ \leftrightarrow O_2^+$	$1 \times 10^{-29} \left(\frac{T_g}{300}\right)^{0.5} \times N_n$	[85]
$O_2 + O^+ \leftrightarrow O + O_2^+$	$2 \times 10^{-11} \left(\frac{T_g}{300}\right)^{-0.4}$	[91,96]
$O_2(a^1\Delta_g) + O^+ \leftrightarrow O + O_2^+$	$2e \times 10^{-11} \left(\frac{T_g}{300}\right)^{-0.5}$	[134]
$O_3 + O^+ \leftrightarrow O_2 + O_2^+$	1×10^{-10}	[91]
$O_2 + C^+ \leftrightarrow CO + O^+$	$0.62 \times 9.9 \times 10^{-10}$	[135]
$O_2 + C^+ \leftrightarrow O + CO^+$	$0.38 \times 9.9 \times 10^{-10}$	[135]
$CO_2 + C^+ \leftrightarrow CO + CO^+$	1.1×10^{-9}	[135]
$C_2O_2^+ \rightarrow CO + CO^+$	$1 \times 10^{-12} \times N_n$	[46]



$O_3^- \rightarrow O_2 + O^-$	$f(E/N)$	[137]
$O + O_3^- \rightarrow O_2 + O_2^-$	$2.5 \times 10^{-10} \left(\frac{T_g}{300}\right)^{0.5}$	[90]
$O + O_3^- \rightarrow O_3 + O^-$	1×10^{-13}	[86]
$O_2(a^1\Delta_g) + O_3^- \leftrightarrow O_2 + O_2 + O^-$	1×10^{-10}	[90]
$O_2(b^1\Sigma_g^+) + O_3^- \rightarrow O_2 + O_2 + O^-$	1×10^{-10}	[90]
$CO_2 + O_3^- \leftrightarrow O_2 + CO_3^-$	$5.5 \times 10^{-10} \left(\frac{T_g}{300}\right)^{-0.49}$	[90,142]
$O(^1D, ^1S) + O_3^- \rightarrow O + O + O_2^-$	1×10^{-10}	[86]
$O(^1D, ^1S) + O_3^- \rightarrow O + O_2 + O^-$	1×10^{-10}	[86]
$O_4^- \rightarrow O_2 + O_2^-$	$1 \times 10^{-10} \times e^{-1044/T_g} \times N_n$	[85]
$O + O_4^- \leftrightarrow O_2 + O_3^-$	4×10^{-10}	[144]
$O + O_4^- \leftrightarrow O_2 + O_2 + O^-$	3×10^{-10}	[85]
$O(^1D, ^1S) + O_4^- \rightarrow O + O_2 + O_2^-$	1×10^{-10}	[86]
$O(^1D, ^1S) + O_4^- \rightarrow O_2 + O_2 + O^-$	1×10^{-10}	[86]
$O_2(a^1\Delta_g) + O_4^- \leftrightarrow O_2 + O_2 + O_2^-$	1×10^{-10}	[90]
$O_2(b^1\Sigma_g^+) + O_4^- \rightarrow O_2 + O_2 + O_2^-$	1×10^{-10}	[90]
$O_3 + O_4^- \leftrightarrow 2O_2 + O_3^-$	3×10^{-10}	[90]
$CO + O_4^- \leftrightarrow O_2 + CO_3^-$	2×10^{-11}	[126]
$CO_2 + O_4^- \rightarrow O_2 + CO_4^-$	3×10^{-10}	[144]
$O + CO_3^- \leftrightarrow CO_2 + O_2^-$	8×10^{-11}	[145,146]
$O(^1D, ^1S) + CO_3^- \rightarrow CO_2 + O + O^-$	1×10^{-10}	[90]
$O + CO_4^- \rightarrow O_2 + CO_3^-$	$0.8 \times 1.4 \times 10^{-10}$	[116,140]

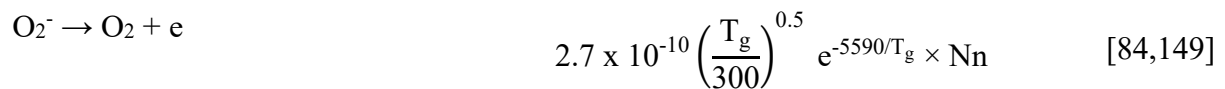
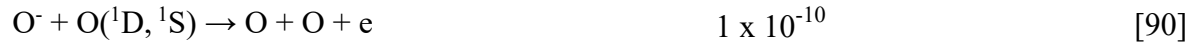
$O + CO_4^- \rightarrow CO_2 + O_2 + O^-$	$0.1 \times 1.4 \times 10^{-10}$	[116,140]
$O + CO_4^- \rightarrow CO_2 + O_3^-$	$0.1 \times 1.4 \times 10^{-10}$	[116,140]
$O(^1D, ^1S) + CO_4^- \rightarrow CO_2 + O + O_2^-$	1×10^{-10}	[90]
$O_2 + CO_4^- \rightarrow CO_2 + O_4^-$	2×10^{-14}	[90]
$O_2(a^1\Delta_g) + CO_4^- \rightarrow CO_2 + O_2 + O_2^-$	1×10^{-10}	[90]
$O_2(b^1\Sigma_g^+) + CO_4^- \rightarrow CO_2 + O_2 + O_2^-$	1×10^{-10}	[90]
$O_3 + CO_4^- \rightarrow CO_2 + O_2 + O_3^-$	4.3×10^{-10}	[138]
$O_3 + CO_4^- \rightarrow O_2 + O_2 + CO_3^-$	3×10^{-11}	[138]
$CO + CO_4^- \rightarrow CO_2 + CO_3^-$	1×10^{-16}	[142]

Ion-ion recombination

$A^- + B^+ \rightarrow A + B$	$2 \times 10^{-7} \left(\frac{T_g}{300}\right)^{-0.5} + 2 \times 10^{-25} \left(\frac{T_g}{300}\right)^{-2.5} \times N_n$	[90,104]
$A^- + B^+ \rightarrow AB$	$1 \times 10^{-25} \left(\frac{T_g}{300}\right)^{-2.5} \times N_n$	[104]
$A^- + BC^+ \rightarrow A + B + C$	1×10^{-7}	[104]
$O^- + O^+ \rightarrow O + O(^1D)$	$4.9 \times 10^{-10} \left(\frac{T_g}{300}\right)^{-0.5}$	[90]
$O^- + O_2^+ \rightarrow O + O_2(a^1\Delta_g)$	$6.3 \times 10^{-10} \left(\frac{T_g}{300}\right)^{-2}$	[86]
$O^- + O_2^+ \rightarrow O + O_2(b^1\Sigma_g^+)$	$1.3 \times 10^{-10} \left(\frac{T_g}{300}\right)^{-2}$	[86]
$O_2^- + O_2^+ \rightarrow O_2 + O_2(a^1\Delta_g)$	$2.9 \times 10^{-10} \left(\frac{T_g}{300}\right)^{-2}$	[86]



Electron detachment



$O_2^- + O_2(b^1\Sigma_g^+) \rightarrow O_2 + O_2 + e$	$3.6 \times 10^{-10} \left(\frac{T_g}{300}\right)^{0.5}$	[86,90]
$O_3^- \rightarrow O_3 + e$	$2.3 \times 10^{-11} \times N_n$	[106]
$O_3^- + O \rightarrow O_2 + O_2 + e$	3×10^{-10}	[86]
$O(^1D, ^1S) + O_3^- \rightarrow O + O_3 + e$	1×10^{-10}	[86]
$O_3 + O_3^- \rightarrow O_2 + O_2 + O_2 + e$	3×10^{-10}	[152]
$CO + O_3^- \rightarrow O_2 + CO_2 + e$	1×10^{-13}	[142,153]
$O(^1D, ^1S) + O_4^- \rightarrow O + 2O_2 + e$	1×10^{-10}	[86]
$O_4^- + O_2(a^1\Delta_g) \rightarrow 3O_2 + e$	1×10^{-10}	[90]
$O_4^- + O_2(b^1\Sigma_g^+) \rightarrow 3O_2 + e$	1×10^{-10}	[90]
$CO_3^- + O \rightarrow CO_2 + O_2 + e$	5×10^{-13}	This study
$CO_3^- + O(^1D, ^1S) \rightarrow CO_2 + 2O + e$	1×10^{-10}	[90]
$CO_3^- + CO \rightarrow 2CO_2 + e$	5×10^{-13}	[47]
$CO_4^- + O(^1D, ^1S) \rightarrow CO_2 + O_2 + O$	1×10^{-10}	[90]
+ e		
$CO_4^- + O_2(a^1\Delta_g) \rightarrow CO_2 + 2O_2 +$	1×10^{-10}	[90]
e		
$CO_4^- + O_2(b^1\Sigma_g^+) \rightarrow CO_2 + 2O_2 +$	1×10^{-10}	[90]
e		

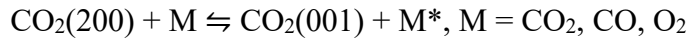
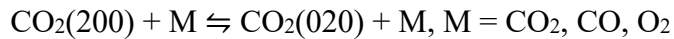
^aexcitation to $v_3 = 2-5$ is included by applying the Fridman scaling [8] and threshold energy shift to the cross sections for $e + CO_2 \leftrightarrow e + CO_2(v_3=1)$, as described in [24].

A2. Details on some rate coefficients for V-T, V-V-T and V-T relaxation

The rate coefficients of intra-molecular V-V-T relaxation are taken from Biondo *et al.* [36], whereas for inter-molecular V-V-T it is taken from Bass [154] as $O_2(i_{02}=1) + CO_2 \leftrightarrow O_2 + CO_2(i_2=2)$ with a forward rate coefficient of $2 \times 10^{-12} \left[\frac{cm^3}{s} \right] (T_g/300[K])^{0.5}$. The reverse rate is computed from the detailed balance principle. The transitions within higher vibrational levels, *i.e.* $i_{02} > 1$ and $i_2 > 2$, are included with the same rate, without applying any scaling law. Finally, $Q_{VT_{12}}$ represents the energy transferred from T_{12} to T_g through V-T relaxation. This term includes the transitions listed in Table A2, taken from the survey of Blauer and Nickerson [57]. The notation used for the vibrational levels involved in the transitions is $CO_2(i_1i_2i_3)$.

Table A2. List of V-T transitions included in $Q_{VT_{12}}$.

V-T transition



*The energy lost from T_{12} corresponds to ϵ_{200} , whereas $\epsilon_{200} - \epsilon_{001}$ is transferred to T_g and ϵ_{001} is transferred to T_3 .

$Q_{VT_{12}}$ contains also V-T relaxation from the bending mode of CO₂ upon collisions with O atoms, with a rate coefficient of $2 \times 10^{-12} \left[\frac{\text{cm}^3}{\text{s}} \right] \cdot \sqrt{T_g/300[\text{K}]}$ taken from Terraz *et al.* [56].

CO₂(00i₃) + CO \rightleftharpoons CO₂ + CO(i_{co}) is taken from [57] with a rate coefficient of $1.66 \times 10^{-24} \left[\frac{\text{cm}^3}{\text{s}} \right] \cdot e^{28.7 - 153 \cdot T_g^{-2/3}}$, while, CO₂(001) + O₂ \rightleftharpoons CO₂(010) + O₂(i_{o2}=1), is included from López-Puertas *et al.* [155], with a rate coefficient of $3 \times 10^{-15} \left[\frac{\text{cm}^3}{\text{s}} \right] \cdot (1 + 0.02 \cdot (T_g - 210))$. Q_{VT_3} includes the transitions listed in Table A3, taken from [57].

Table A3. List of V-T transitions included in Q_{VT_3} .

V-T transition



In addition to those listed in Table A3, Q_{VT_3} incorporates also V-T deactivation by collisions with O atoms, CO₂(001) + O \rightleftharpoons CO₂(0i₂0) + O, with i₂ = 1, 2, 3 and 4. The rate coefficient for this transition is $2 \times 10^{-13} \left[\frac{\text{cm}^3}{\text{s}} \right] \cdot \sqrt{T_g/300[\text{K}]}$ and assumed independent of i₂ [56].

We would like to point out that all rate coefficients for CO₂ V-T and intra-molecular V-V-T relaxation involving higher vibrational levels are scaled based on the Schwartz–Slawsky–Herzfeld (SSH) theory [24,36].

References

- [1] Wei M, McMillan C A and De La Rue Du Can S 2019 Electrification of Industry: Potential, Challenges and Outlook *Curr Sustainable Renewable Energy Rep* **6** 140–8
- [2] Shuka P R and III I P on C C W G 2022 *Climate Change 2022: Mitigation of Climate Change : Working Group III Contribution to the Sixth Assessment Report of the Intergovernmental Panel on Climate Change* (Cambridge University Press)
- [3] Mallapragada D S, Dvorkin Y, Modestino M A, Esposito D V, Smith W A, Hodge B-M, Harold M P, Donnelly V M, Nuz A, Bloomquist C, Baker K, Grabow L C, Yan Y, Rajput N N, Hartman R L, Biddinger E J, Aydil E S and Taylor A D 2023 Decarbonization of the chemical industry through electrification: Barriers and opportunities *Joule* **7** 23–41
- [4] Snoeckx R and Bogaerts A 2017 Plasma technology – a novel solution for CO₂ conversion? *Chem. Soc. Rev.* **46** 5805–63
- [5] Bogaerts A and Neyts E C 2018 Plasma Technology: An Emerging Technology for Energy Storage *ACS Energy Lett.* **3** 1013–27
- [6] Osorio-Tejada J, Escriba-Gelonch M, Vertongen R, Bogaerts A and Hessel V 2024 CO₂ conversion to CO via plasma and electrolysis: a techno-economic and energy cost analysis *Energy Environ. Sci.* 10.1039.D4EE00164H
- [7] Rabinovich A, Nirenberg G, Kocagoz S, Surace M, Sales C and Fridman A 2022 Scaling Up of Non-Thermal Gliding Arc Plasma Systems for Industrial Applications *Plasma Chem Plasma Process* **42** 35–50
- [8] Fridman A 2008 *Plasma Chemistry* (Cambridge: Cambridge University Press)
- [9] Rivallan M, Aiello S and Thibault-Starzyk F 2010 Microsecond time-resolved Fourier transform infrared analytics in a low pressure glow discharge reactor *Review of Scientific Instruments* **81** 103111
- [10] Klarenaar B L M, Engeln R, van den Bekerom D C M, van de Sanden M C M, Morillo-Candas A S and Guitella O 2017 Time evolution of vibrational temperatures in a CO₂ glow discharge measured with infrared absorption spectroscopy *Plasma Sources Sci. Technol.* **26** 115008
- [11] Amat G and Pimbert M 1965 On Fermi resonance in carbon dioxide *Journal of Molecular Spectroscopy* **16** 278–90
- [12] Jacobs R R, Pettipiece K J and Thomas S J 1974 Rotational relaxation rate constants for CO₂ *Applied Physics Letters* **24** 375–7
- [13] Dang C, Reid J and Garside B K 1982 Detailed vibrational population distributions in a CO₂ laser discharge as measured with a tunable diode laser *Appl. Phys. B* **27** 145–51
- [14] Klarenaar B L M, Grofulović M, Morillo-Candas A S, Bekerom D C M van den, Damen M A, Sanden M C M van de, Guitella O and Engeln R 2018 A rotational Raman study under non-thermal conditions in a pulsed CO₂ glow discharge *Plasma Sources Sci. Technol.* **27** 045009

- [15] Van Den Bekerom D C M, Palomares Linares J M, Van Veldhuizen E M, Nijdam S, Van De Sanden M C M and Van Rooij G J 2018 How the alternating degeneracy in rotational Raman spectra of CO₂ and C₂H₂ reveals the vibrational temperature *Appl. Opt.* **57** 5694
- [16] Klarenaar B L M, Morillo-Candas A S, Grofulović M, Sanden M C M V D, Engeln R and Guaitella O 2019 Excitation and relaxation of the asymmetric stretch mode of CO₂ in a pulsed glow discharge *Plasma Sources Sci. Technol.* **28** 035011
- [17] Damen M A, Martini L M and Engeln R 2020 Temperature evolution in a pulsed CO₂-N₂ glow discharge measured using quantum cascade laser absorption spectroscopy *Plasma Sources Sci. Technol.* **29** 065016
- [18] Damen M A, Martini L M and Engeln R 2020 Vibrational quenching by water in a CO₂ glow discharge measured using quantum cascade laser absorption spectroscopy *Plasma Sources Sci. Technol.* **29** 095017
- [19] Vervloedt S C L, Budde M and Engeln R 2023 Influence of oxygen on the ro-vibrational kinetics of a non-equilibrium discharge in CO₂-O₂ mixtures *Plasma Sources Sci. Technol.* **32** 015004
- [20] Raizer Y P 1991 *Gas Discharge Physics* ed J E Allen (Berlin, Heidelberg: Springer Berlin Heidelberg)
- [21] Hurlbatt A, Gibson A R, Schröter S, Bredin J, Foote A P S, Grondein P, O'Connell D and Gans T 2017 Concepts, Capabilities, and Limitations of Global Models: A Review *Plasma Processes & Polymers* **14** 1600138
- [22] Alves L L, Bogaerts A, Guerra V and Turner M M 2018 Foundations of modelling of nonequilibrium low-temperature plasmas *Plasma Sources Sci. Technol.* **27** 023002
- [23] Aerts R, Martens T and Bogaerts A 2012 Influence of Vibrational States on CO₂ Splitting by Dielectric Barrier Discharges *J. Phys. Chem. C* **116** 23257–73
- [24] Kozák T and Bogaerts A 2014 Splitting of CO₂ by vibrational excitation in non-equilibrium plasmas: a reaction kinetics model *Plasma Sources Sci. Technol.* **23** 045004
- [25] Treanor C E 1965 Vibrational Energy Transfer in High-Energy Collisions *The Journal of Chemical Physics* **43** 532–8
- [26] Kozák T and Bogaerts A 2014 Evaluation of the energy efficiency of CO₂ conversion in microwave discharges using a reaction kinetics model *Plasma Sources Sci. Technol.* **24** 015024
- [27] Berthelot A and Bogaerts A 2016 Modeling of plasma-based CO₂ conversion: lumping of the vibrational levels *Plasma Sources Sci. Technol.* **25** 045022
- [28] Berthelot A and Bogaerts A 2017 Modeling of CO₂ Splitting in a Microwave Plasma: How to Improve the Conversion and Energy Efficiency *J. Phys. Chem. C* **121** 8236–51
- [29] Kabouzi Y, Calzada M D, Moisan M, Tran K C and Trassy C 2002 Radial contraction of microwave-sustained plasma columns at atmospheric pressure *Journal of Applied Physics* **91** 1008–19

- [30] Silva T, Grofulović M, Klarenaar B L M, Morillo-Candas A S, Guaitella O, Engeln R, Pintassilgo C D and Guerra V 2018 Kinetic study of low-temperature CO₂ plasmas under non-equilibrium conditions. I. Relaxation of vibrational energy *Plasma Sources Sci. Technol.* **27** 015019
- [31] Grofulović M, Silva T, Klarenaar B L M, Morillo-Candas A S, Guaitella O, Engeln R, Pintassilgo C D and Guerra V 2018 Kinetic study of CO₂ plasmas under non-equilibrium conditions. II. Input of vibrational energy *Plasma Sources Sci. Technol.* **27** 115009
- [32] Silva T, Grofulović M, Terraz L, Pintassilgo C D and Guerra V 2020 Dynamics of Gas Heating in the Afterglow of Pulsed CO₂ and CO₂-N₂ Glow Discharges at Low Pressure *Plasma Chem Plasma Process* **40** 713–25
- [33] Kotov V 2022 Vibrational relaxation and triggering of the non-equilibrium vibrational decomposition of CO₂ in gas discharges *Plasma Sources Sci. Technol.* **31** 094002
- [34] Kotov V 2021 Two-modes model of the non-equilibrium plasma chemical dissociation of CO₂ *Plasma Sources Sci. Technol.* **30** 055003
- [35] Pietanza L D, Colonna G and Capitelli M 2022 Non-equilibrium plasma kinetics of CO₂ in glow discharges: a comparison with existing modeling and experimental results *Plasma Sources Sci. Technol.* **31** 104001
- [36] Biondo O, Fromentin C, Silva T, Guerra V, Van Rooij G and Bogaerts A 2022 Insights into the limitations to vibrational excitation of CO₂: validation of a kinetic model with pulsed glow discharge experiments *Plasma Sources Sci. Technol.* **31** 074003
- [37] Smith K and Thomson R M 1978 *Computer Modeling of Gas Lasers* (Boston, MA: Springer US)
- [38] Kustova E V and Nagnibeda E A 2006 On a correct description of a multi-temperature dissociating CO₂ flow *Chemical Physics* **321** 293–310
- [39] Kustova E, Mekhonoshina M and Kosareva A 2019 Relaxation processes in carbon dioxide *Physics of Fluids* **31** 046104
- [40] Kunova O, Kosareva A, Kustova E and Nagnibeda E 2020 Vibrational relaxation of carbon dioxide in state-to-state and multi-temperature approaches *Phys. Rev. Fluids* **5** 123401
- [41] Kustova E and Mekhonoshina M 2021 Novel approach for evaluation of CO₂ vibrational relaxation times *Chemical Physics Letters* **764** 138288
- [42] Adamovich I V, Macheret S O, Rich J W and Treanor C E 1998 Vibrational Energy Transfer Rates Using a Forced Harmonic Oscillator Model *Journal of Thermophysics and Heat Transfer* **12** 57–65
- [43] Anon COMSOL Multiphysics® v. 6.2.
- [44] Pietanza L D, Colonna G and Capitelli M 2024 Self-Consistent State-to-State Kinetic Modeling of CO₂ Cold Plasmas: Insights on the Role of Electronically Excited States *Plasma Chem Plasma Process* **44** 1431–68

- [45] Koelman P, Heijkers S, Tadayon Mousavi S, Graef W, Mihailova D, Kozak T, Bogaerts A and Van Dijk J 2017 A Comprehensive Chemical Model for the Splitting of CO₂ in Non-Equilibrium Plasmas *Plasma Processes & Polymers* **14** 1600155
- [46] Cenian A, Chernukho A and Borodin V 1995 Modeling of Plasma-Chemical Reactions in Gas Mixture of CO₂ lasers. II. Theoretical Model and its Verification *Contrib. Plasma Phys.* **35** 273–96
- [47] Shields H, Smith A L S and Norris B 1976 Negative ion effects in TEA CO₂ lasers *J. Phys. D: Appl. Phys.* **9** 1587–603
- [48] Phelps A V 1990 The diffusion of charged particles in collisional plasmas: Free and ambipolar diffusion at low and moderate pressures *J. RES. NATL. INST. STAN.* **95** 407
- [49] Silva A F, Morillo-Candás A S, Tejero-del-Caz A, Alves L L, Guaitella O and Guerra V 2020 A reaction mechanism for vibrationally-cold low-pressure CO₂ plasmas *Plasma Sources Sci. Technol.* **29** 125020
- [50] Guerra V and Loureiro J 1997 Self-consistent electron and heavy-particle kinetics in a low-pressure - glow discharge *Plasma Sources Sci. Technol.* **6** 373–85
- [51] Ellis H W, Pai R Y, McDaniel E W, Mason E A and Viehland L A 1976 Transport properties of gaseous ions over a wide energy range *Atomic Data and Nuclear Data Tables* **17** 177–210
- [52] Cenian A 1989 Study of nonequilibrium vibrational relaxation of CO₂ molecules during adiabatic expansion in a supersonic nozzle. The treanor type distribution - existence and generation *Chemical Physics* **132** 41–8
- [53] Marrone P V and Treanor C E 1963 Chemical Relaxation with Preferential Dissociation from Excited Vibrational Levels *The Physics of Fluids* **6** 1215–21
- [54] Kosareva A, Kunova O, Kustova E and Nagnibeda E 2022 Hybrid approach to accurate modeling of coupled vibrational-chemical kinetics in carbon dioxide *Physics of Fluids* **34** 026105
- [55] Pintassilgo C D, Guerra V, Guaitella O and Rousseau A 2014 Study of gas heating mechanisms in millisecond pulsed discharges and afterglows in air at low pressures *Plasma Sources Sci. Technol.* **23** 025006
- [56] Terraz L, Silva T, Morillo-Candas A, Guaitella O, Tejero-del-Caz A, Alves L L and Guerra V 2020 Influence of N₂ on the CO₂ vibrational distribution function and dissociation yield in non-equilibrium plasmas *J. Phys. D: Appl. Phys.* **53** 094002
- [57] Blauer J and Nickerson G 1974 A survey of vibrational relaxation rate data for processes important to CO₂-N₂-H₂O infrared plume radiation *7th Fluid and Plasma Dynamics Conference 7th Fluid and Plasma Dynamics Conference (Palo Alto, CA, U.S.A.: American Institute of Aeronautics and Astronautics)*
- [58] Fromentin C, Silva T, Dias T C, Morillo-Candas A S, Biondo O, Guaitella O and Guerra V 2023 Study of vibrational kinetics of CO₂ and CO in CO₂-O₂ plasmas under non-equilibrium conditions *Plasma Sources Sci. Technol.* **32** 024001

- [59] Fromentin C, Silva T, Dias T C, Baratte E, Guaitella O and Guerra V 2023 Validation of non-equilibrium kinetics in CO₂-N₂ plasmas *Plasma Sources Sci. Technol.* **32** 054004
- [60] Thomson R M 1978 The thermal conductivity of gases with vibrational internal energy *J. Phys. D: Appl. Phys.* **11** 2509–16
- [61] Eucken A 1913 On the thermal conductivity, the specific heat and the viscosity of gases *Physikalische Zeitschrift* **14** 324–33
- [62] Neufeld P D, Janzen A R and Aziz R A 1972 Empirical Equations to Calculate 16 of the Transport Collision Integrals $\Omega(l, s)^*$ for the Lennard-Jones (12–6) Potential *The Journal of Chemical Physics* **57** 1100–2
- [63] Brokaw R S 1969 Predicting Transport Properties of Dilute Gases *Ind. Eng. Chem. Proc. Des. Dev.* **8** 240–53
- [64] Anon 2023 Plasma Module User's Guide, pp. 120, COMSOL Multiphysics® v. 6.2
- [65] Kee R J, Coltrin M E and Glarborg P 2003 *Chemically Reacting Flow: Theory and Practice* (Wiley)
- [66] Maerivoet S, Tsonev I, Slaets J, Reniers F and Bogaerts A 2024 Coupled multi-dimensional modelling of warm plasmas: Application and validation for an atmospheric pressure glow discharge in CO₂/CH₄/O₂ *Chemical Engineering Journal* **492** 152006
- [67] McBride B J, Zehe M J and Sanford G 2002 NASA Glenn Coefficients for Calculating Thermodynamic Properties of Individual Species
- [68] Goos E, Burcat A and Ruscic B EXTENDED THIRD MILLENNIUM IDEAL GAS AND CONDENSED PHASE THERMOCHEMICAL DATABASE FOR COMBUSTION WITH UPDATES FROM ACTIVE THERMOCHEMICAL TABLES
- [69] Illies A J 1988 Thermochemistry for the gas-phase ion-molecule clustering of CO₂+CO₂, SO₂+CO₂, N₂O+N₂O, O₂+CO₂, NO+CO₂, O₂+N₂O and NO+N₂O: description of a new hybrid drift tube/ion source with coaxial electron beam and ion exit apertures *J. Phys. Chem.* **92** 2889–96
- [70] Linstrom P 1997 NIST Chemistry WebBook, NIST Standard Reference Database 69
- [71] Rusanov V D, Fridman A A and Sholin G V 1981 The physics of a chemically active plasma with nonequilibrium vibrational excitation of molecules *Sov. Phys. Usp.* **24** 447–74
- [72] Vermeiren V and Bogaerts A 2019 Improving the Energy Efficiency of CO₂ Conversion in Nonequilibrium Plasmas through Pulsing *J. Phys. Chem. C* **123** 17650–65
- [73] Nagnibeda E and Kustova E 2009 *Non-Equilibrium Reacting Gas Flows* (Berlin, Heidelberg: Springer Berlin Heidelberg)
- [74] Moruzzi J L and Phelps A V 1966 Survey of Negative-Ion—Molecule Reactions in O₂, CO₂, H₂O, CO, and Mixtures of These Gases at High Pressures *The Journal of Chemical Physics* **45** 4617–27

- [75] Ranjan R and Goodyear C C 1973 Collisional detachment from atmospheric negative ions *J. Phys. B: At. Mol. Phys.* **6** 1070–8
- [76] Naidis G V and Babaeva N Yu 2022 Modeling of repetitively pulsed low-pressure CO₂ discharges *Physics of Plasmas* **29** 044501
- [77] Paulson J F, Dale F and Mosher R L 1964 Production of C₂O₄⁺ in an Ion-molecule Reaction *Nature* **204** 377–8
- [78] Rakshit A B and Warneck P 1981 Formation and reactions of O₂⁺·CO₂, O₂⁺·H₂O and O₂⁺·(CO₂)₂ ions *International Journal of Mass Spectrometry and Ion Physics* **40** 135–55
- [79] Alves L L 2014 The IST-LISBON database on LXCat *J. Phys.: Conf. Ser.* **565** 012007
- [80] Polak L S and Slovetsky D I 1976 Electron impact induced electronic excitation and molecular dissociation *International Journal for Radiation Physics and Chemistry* **8** 257–82
- [81] Ogloblina P, Tejero-del-Caz A, Guerra V and Alves L L 2020 Electron impact cross sections for carbon monoxide and their importance in the electron kinetics of CO₂–CO mixtures *Plasma Sources Sci. Technol.* **29** 015002
- [82] Gousset G, Ferreira C M, Pinheiro M, Sa P A, Touzeau M, Vialle M and Loureiro J 1991 Electron and heavy-particle kinetics in the low pressure oxygen positive column *J. Phys. D: Appl. Phys.* **24** 290–300
- [83] Alves L L, Coche P, Ridenti M A and Guerra V 2016 Electron scattering cross sections for the modelling of oxygen-containing plasmas* *Eur. Phys. J. D* **70** 124
- [84] Pack J L and Phelps A V 1966 Electron Attachment and Detachment. I. Pure O₂ at Low Energy *The Journal of Chemical Physics* **44** 1870–83
- [85] Kossyi I A, Kostinsky A Y, Matveyev A A and Silakov V P 1992 Kinetic scheme of the non-equilibrium discharge in nitrogen-oxygen mixtures *Plasma Sources Sci. Technol.* **1** 207–20
- [86] Feoktistov V A, Mukhovatova A V, Popov A M and Rakhimova T V 1995 Self-consistent modelling of low-pressure RF discharges in oxygen plasma *J. Phys. D: Appl. Phys.* **28** 1346–83
- [87] Morgan L W Morgan (Kinema Research & Software)
- [88] Wang Y, Zatsarinny O and Bartschat K 2013 B-spline R-matrix-with-pseudostates calculations for electron-impact excitation and ionization of carbon *Phys. Rev. A* **87** 012704
- [89] Donovan R J and Husain D 1967 Vibrational excitation of carbon monoxide following quenching of the a³ state *Trans. Faraday Soc.* **63** 2879
- [90] Murakami T, Niemi K, Gans T, O'Connell D and Graham W G 2012 Chemical kinetics and reactive species in atmospheric pressure helium–oxygen plasmas with humid-air impurities *Plasma Sources Sci. Technol.* **22** 015003

- [91] Zinn J, Sutherland C D, Stone S N, Duncan L M and Behnke R 1982 Ionospheric effects of rocket exhaust products—heao-c, skylab *Journal of Atmospheric and Terrestrial Physics* **44** 1143–71
- [92] Cobos C, Castellano E and Schumacher H J 1983 The kinetics and the mechanism of ozone photolysis at 253.7 nm *Journal of Photochemistry* **21** 291–312
- [93] Baulch D L, Cox R A, Hampson R F, Kerr (Chairman) J A, Troe J and Watson R T 1984 Evaluated Kinetic and Photochemical Data for Atmospheric Chemistry: Supplement II. CODATA Task Group on Gas Phase Chemical Kinetics *Journal of Physical and Chemical Reference Data* **13** 1259–380
- [94] Tully J C 1975 Reactions of O(¹D) with atmospheric molecules *The Journal of Chemical Physics* **62** 1893–8
- [95] Sedlacek A J, Harding D R, Weston R E, Kreutz T G and Flynn G W 1989 Probing the O(1D)+CO₂ reaction with second-derivative modulated diode laser spectroscopy *The Journal of Chemical Physics* **91** 7550–6
- [96] Bortner M and Baurer T 1978 Defense Nuclear Agency reaction rate hand-book, Revision number 7 *Unknown*
- [97] Black G, Sharpless R L, Slanger T G and Lorents D C 1975 Quantum yields for the production of O(1S), N(2D), and N₂(A 3Σ⁺ u) from the vacuum uv photolysis of N₂O *The Journal of Chemical Physics* **62** 4266–73
- [98] Slanger T G and Black G 1978 O(1S) interactions—the product channels *The Journal of Chemical Physics* **68** 989–97
- [99] Capetanakis F P, Sondermann F, Höser S and Stuhl F 1993 Temperature dependence of the quenching of O(1S) by simple inorganic molecules *The Journal of Chemical Physics* **98** 7883–7
- [100] Stuhl F and Welge K H 1969 Deactivation of O(¹S) and O₂(^b1Σ_g⁺) *Can. J. Chem.* **47** 1870–7
- [101] Slanger T G and Black G 1976 O(1S) quenching by O(3P) *The Journal of Chemical Physics* **64** 3763–6
- [102] Hampson R F, Garvin D, Transportation U S D of and Standards U S N B of 1978 *Reaction Rate and Photochemical Data for Atmospheric Chemistry, 1977* (U.S. Department of Commerce, National Bureau of Standards)
- [103] Didyukov A I, Kulagin Y A, Shelepin L A and Yarygina V N 1989 Analysis of the rates of the processes involving singlet oxygen molecules *Sov. J. Quantum Electron.* **19** 578–87
- [104] Gordiets B F, Ferreira C M, Guerra V L, Loureiro J M A H, Nahorny J, Pagnon D, Touzeau M and Vialle M 1995 Kinetic model of a low-pressure N/sub 2/-O/sub 2/ flowing glow discharge *IEEE Trans. Plasma Sci.* **23** 750–68
- [105] Vasiljeva A N, Klopovskiy K S, Kovalev A S, Lopaev D V, Mankelevich Y A, Popov N A, Rakhimov A T and Rakhimova T V 2004 On the possibility of O₂(^a1_g) production by a non-self-sustained discharge for oxygen–iodine laser pumping *J. Phys. D: Appl. Phys.* **37** 2455–68

- [106] Gudmundsson J T and Thorsteinsson E G 2007 Oxygen discharges diluted with argon: dissociation processes *Plasma Sources Sci. Technol.* **16** 399–412
- [107] Sharipov A and Starik A 2011 Theoretical Study of the Reaction of Carbon Monoxide with Oxygen Molecules in the Ground Triplet and Singlet Delta States *J. Phys. Chem. A* **115** 1795–803
- [108] Hesser J E and Dressler K 1966 Radiative Lifetimes of Ultraviolet Molecular Transitions *The Journal of Chemical Physics* **45** 3149–50
- [109] Schwenker R P 1965 Experimental Oscillator Strengths of CO and CO+ *The Journal of Chemical Physics* **42** 1895–7
- [110] Moore J H and Robinson D W 1968 Study of Some Electronic Transition Probabilities in CO and CN *The Journal of Chemical Physics* **48** 4870–4
- [111] Smith G P, Golden D M, Frenklach M, Moriarty N W, Eiteneer B, Goldenberg M, Bowman T C, Hanson R K, Song S, Gardiner W C Jr, Lissianski V V and Qin Z GRI-Mech 3.0
- [112] Viggiano A A, Ehlerding A, Hellberg F, Thomas R D, Zhaunerchyk V, Geppert W D, Montaigne H, Larsson M, Kaminska M and Österdahl F 2005 Rate constants and branching ratios for the dissociative recombination of CO₂⁺ *The Journal of Chemical Physics* **122** 226101
- [113] Popov N A and Starikovskaia S M 2022 Relaxation of electronic excitation in nitrogen/oxygen and fuel/air mixtures: fast gas heating in plasma-assisted ignition and flame stabilization *Progress in Energy and Combustion Science* 100928
- [114] Guðmundsson J T and Lieberman M *Recombination rate coefficients in oxygen discharges* (Science Institute, University of Iceland)
- [115] Rosén S, Peverall R, Larsson M, Le Padellec A, Semaniak J, Larson Å, Strömholm C, Van Der Zande W J, Danared H and Dunn G H 1998 Absolute cross sections and final-state distributions for dissociative recombination and excitation of CO⁺ (v = 0) using an ion storage ring *Phys. Rev. A* **57** 4462–71
- [116] Thomas G. Beuthe T G B and Jen-Shih Chang J-S C 1997 Chemical Kinetic Modelling of Non-Equilibrium Ar-CO₂ Thermal Plasmas *Jpn. J. Appl. Phys.* **36** 4997
- [117] Whitaker M, Biondi M A and Johnsen R 1981 Electron-temperature dependence of dissociative recombination of electrons with C O + · (CO) n -series ions *Phys. Rev. A* **23** 1481–5
- [118] Sennhauser E S, Armstrong D A and Warman J M 1980 The temperature dependence of three-body electron ion recombination in gaseous H₂O, NH₃ and CO₂ *Radiation Physics and Chemistry (1977)* **15** 479–83
- [119] Babaeva N Yu and Naidis G V 2001 On streamer dynamics in dense media *Journal of Electrostatics* **53** 123–33

- [120] Aleksandrov N L, Kindysheva S V, Kirpichnikov A A, Kosarev I N, Starikovskaia S M and Starikovskii A Y 2007 Plasma decay in N_2 , CO_2 and H_2O excited by high-voltage nanosecond discharge *J. Phys. D: Appl. Phys.* **40** 4493–502
- [121] Fehsenfeld F C, Dunkin D B and Ferguson E E 1970 Rate constants for the reaction of CO_2^+ with O, O_2 and NO; N_2^+ with O and NO; and O_2^+ with NO *Planetary and Space Science* **18** 1267–9
- [122] Ferguson E E, Van Dorenai J M, Viggiano A A, Morris R A, Paulson J F, Stewart J D, Sunderlin L S and Armentrout P B 1992 Internal and translational energy effects on the charge-transfer reaction of CO_2^+ with O_2 *International Journal of Mass Spectrometry and Ion Processes* **117** 261–82
- [123] Fox J L, Benna M, McFadden J P and Jakosky B M 2021 Rate coefficients for the reactions of CO_2^+ with O: Lessons from MAVEN at Mars *Icarus* **358** 114186
- [124] Coxon P and Moruzzi J L 1977 Ion-molecule reactions in CO_2 and CO_2 -CO mixtures *J. Phys. D: Appl. Phys.* **10** 969–77
- [125] Prasad S S and Huntress W T Jr 1980 A model for gas phase chemistry in interstellar clouds. I - The basic model, library of chemical reactions, and chemistry among C, N, and O compounds *ApJS* **43** 1
- [126] Adams N G, Bohme D K, Dunkin D B, Fehsenfeld F C and Ferguson E E 1970 Flowing Afterglow Studies of Formation and Reactions of Cluster Ions of O_2^+ , O_2^- , and O^- *The Journal of Chemical Physics* **52** 3133–40
- [127] Smith D, Adams N G and Miller T M 1978 A laboratory study of the reactions of N^+ , N_2^+ , N_3^+ , N_4^+ , O^+ , O_2^+ , and NO^+ ions with several molecules at 300 K *The Journal of Chemical Physics* **69** 308–18
- [128] Rakshit A and Warneck P 1980 Routes to the formation of association products in CO_2 from reactions of CO_2^- CO_2^+ ions with several neutral molecules *Zeitschrift für Naturforschung A* **35** 358–60
- [129] Adams N G, Smith D and Grief D 1978 Reactions of $HnCO^+$ ions with molecules at 300 K *International Journal of Mass Spectrometry and Ion Physics* **26** 405–15
- [130] Miller T M, Wetterskog R E and Paulson J F 1984 Temperature dependence of the ion-molecule reactions $N^{++}CO$, $C^{++}NO$, and C^+ , CO^+ , CO_2^+ O_2 from 90–450 K *The Journal of Chemical Physics* **80** 4922–5
- [131] Fehsenfeld F C and Ferguson E E 1972 Thermal Energy Reaction Rate Constants for H^+ and CO^+ with O and NO *The Journal of Chemical Physics* **56** 3066–70
- [132] Chong S-L and Franklin J L 1971 High-Pressure Ion-Molecule Reactions in Carbon Monoxide and Carbon Monoxide-Methane Mixtures *The Journal of Chemical Physics* **54** 1487–95
- [133] Sieck L W and Gorden R 1974 Photoionization of CO_2 - CO - O_2 mixtures. Formation and reactions of ion clusters *J. RES. NATL. BUR. STAN. SECT. A.* **78A** 315
- [134] Dias T C, Fromentin C, Alves L L, Tejero-del-Caz A, Silva T and Guerra V 2023 A reaction mechanism for oxygen plasmas *Plasma Sources Sci. Technol.* **32** 084003

- [135] Smith D and Adams N G 1977 Reaction of simple hydrocarbon ions with molecules at thermal energies *International Journal of Mass Spectrometry and Ion Physics* **23** 123–35
- [136] Sieck L W 1978 Reactions of $(\text{CO}_2)_2^+$ and $(\text{CO})_2^+$ association ions *Int J of Chemical Kinetics* **10** 335–66
- [137] Kinsman P R and Rees J A 1970 Ionization, attachment and ion—Molecule reactions in oxygen *International Journal of Mass Spectrometry and Ion Physics* **5** 71–81
- [138] Williams S, Campos M F, Midey A J, Arnold S T, Morris R A and Viggiano A A 2002 Negative Ion Chemistry of Ozone in the Gas Phase *J. Phys. Chem. A* **106** 997–1003
- [139] Zymak I, Žabka J, Polášek M, Tran T D, Španěl P and Smith D 2021 Experimental study of the reaction of O^- ions with CO_2 molecules with different ternary gases at temperatures relevant to the martian ionosphere *Icarus* **354** 114057
- [140] Albritton D L 1978 Ion-neutral reaction-rate constants measured in flow reactors through 1977 *Atomic Data and Nuclear Data Tables* **22** 1–89
- [141] Lifshitz C, Wu R L C, Tiernan T O and Terwilliger D T 1978 Negative ion—molecule reactions of ozone and their implications on the thermochemistry of O_3^- *The Journal of Chemical Physics* **68** 247–60
- [142] Parkes D A 1973 Oxygen negative ion reactions with carbon dioxide and carbon monoxide. Part 2 *J. Chem. Soc., Faraday Trans. 1* **69** 198
- [143] Fehsenfeld F C and Ferguson E E 1974 Laboratory studies of negative ion reactions with atmospheric trace constituents *The Journal of Chemical Physics* **61** 3181–93
- [144] Fehsenfeld F C, Ferguson E E and Bohme D K 1969 Additional flowing afterglow measurements of negative ion reactions of D-region interest *Planetary and Space Science* **17** 1759–62
- [145] Fehsenfeld F C, Schmeltekopf A L, Schiff H I and Ferguson E E 1967 Laboratory measurements of negative ion reactions of atmospheric interest *Planetary and Space Science* **15** 373–9
- [146] Niles F E 1970 Airlike Discharges with CO_2 , NO , NO_2 , and N_2O as Impurities *The Journal of Chemical Physics* **52** 408–24
- [147] Cenian A, Chernukho A, Borodin V and Śliwiński G 1994 Modeling of Plasma-Chemical Reactions in Gas Mixture of CO_2 Lasers I. Gas Decomposition in Pure CO_2 Glow Discharge *Contrib. Plasma Phys.* **34** 25–37
- [148] Frommhold L 1964 Über verzögerte Elektronen in Elektronenlawinen, insbesondere in Sauerstoff und Luft, durch Bildung und Zerfall negativer Ionen (O^-) *Fortschr. Phys.* **12** 597–642
- [149] Phelps A V 1969 Laboratory studies of electron attachment and detachment processes of aeronomic interest *Can. J. Chem.* **47** 1783–93

- [150] McFarland M, Albritton D L, Fehsenfeld F C, Ferguson E E and Schmeltekopf A L 1973 Flow-drift technique for ion mobility and ion-molecule reaction rate constant measurements. III. Negative ion reactions of O^- with CO, NO, H_2 , and D_2 *The Journal of Chemical Physics* **59** 6629–35
- [151] Fehsenfeld F C, Albritton D L, Burt J A and Schiff H I 1969 Associative-detachment reactions of O^- and O_2^- by $O_2(^1\Delta_g)$ *Can. J. Chem.* **47** 1793–5
- [152] Khvorostovskaya L E and Yankovsky V A 1991 Negative Ions, Ozone, and Metastable Components in dc Oxygen Glow Discharge *Contrib. Plasma Phys.* **31** 71–88
- [153] Willis C and Boyd A W 1976 Excitation in the radiation chemistry of inorganic gases *International Journal for Radiation Physics and Chemistry* **8** 71–111
- [154] Bass H E 1973 Vibrational relaxation in CO_2/O_2 mixtures *The Journal of Chemical Physics* **58** 4783–6
- [155] López-Puertas M, Rodrigo R, López-Moreno J J and Taylor F W 1986 A non-LTE radiative transfer model for infrared bands in the middle atmosphere. II. CO_2 (2.7 and 4.3 μm) and water vapour (6.3 μm) bands and $N_2(1)$ and $O_2(1)$ vibrational levels *Journal of Atmospheric and Terrestrial Physics* **48** 749–64